ACS Catalysis

pubs.acs.org/acscatalysis Research Article

Catalytic Consequences of Hierarchical Pore Architectures within MFI and FAU Zeolites for Polyethylene Conversion

Jun Zhi Tan, Maaso Ortega, Sophia A. Miller, Cole W. Hullfish, Hojoon Kim, Sungmin Kim, Wenda Hu, Jian Zhi Hu, Johannes A. Lercher, Bruce E. Koel, and Michele L. Sarazen*

Cite This: ACS Catal. 2024, 14, 7536–7552 Read Online

ACCESS | Metrics & More | Article Recommendations | Supporting Information

ABSTRACT: The benefits of hierarchical zeolites for the conversion of bulky molecules like polymeric waste have been reported in the literature; however, the impact of mesopore sizes and connectivities on rates, product selectivities, and catalyst deactivation in the context of plastic upcycling has not been systematically probed. Here, we synthesized a suite of hierarchical MFI and FAU zeolites via desilication under varying conditions for metal-free polyethylene conversion reactions under batch and flow conditions (473−523 K). Polyethylene (solid) conversion rates (normalized by Brønsted acid site density) were higher on hierarchical than parent microporous MFI regardless of mesopore connectivities, i.e., open or constricted, suggesting that the incorporation of mesopores facilitates diffusion of intermediate products to access medium-pore protons for successive scission events. Furthermore, higher branched:linear gaseous product ratios were produced on hierarchical than parent MFI, since mesopores allow for egress of bulkier molecules without undergoing further secondary events, e.g., isomerization back to linear alkanes/alkenes or beta scission. Solid conversion rates on hierarchical FAU synthesized via desilication with cetyltrimethylammonium bromide (CTABr), however, were not higher than parent FAU, likely because the presence of CTABr facilitates recrystallization of leached species to form composites (hierarchical FAU and ordered mesoporous materials) with more isolated mesopores. The stagnation in rates, despite increased mesopore volumes (>0.22 $cm^3\ g^{-1}$), highlights the importance of confinement effects provided by micropores for cleaving C−C bonds at modest reaction conditions. *In situ* ^1H MAS NMR performed on polyethylene with MFI zeolite show that PE isomerizes (and potentially deconstructs) at temperatures near 450 K, highlighting the role of Brønsted acid sites in activating C−C bonds under mild reaction conditions. Catalyst recyclability studies showed that all catalysts undergo deactivation during plastic upcycling reactions, but to varying extents. Overall, hierarchical materials have better catalyst stability than parent materials, although the differences in stability between hierarchical and parent FAU are smaller than those for MFI. Taken together, these findings demonstrate how rates, selectivities, and catalyst deactivation from plastic upcycling reactions can be controlled via fine-tuning the identity and connectivity of mesopores.

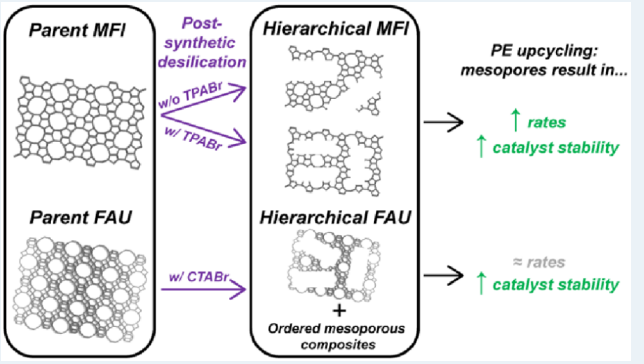

KEYWORDS: *polyolefin conversion, hierarchical zeolites, catalyst deactivation, solid acid catalysis, postsynthetic modification*

Downloaded via PACIFIC NORTHWEST NATL LABORATORY on May 14, 2024 at 22:29:55 (UTC).
See https://pubs.acs.org/sharingguidelines for options on how to legitimately share published articles.

1. INTRODUCTION

Plastics are extensively used across different industries due to their versatility in a multitude of applications.[1] The societal benefits of plastics, however, are countered by the detrimental effects of their pollution of natural environments.[2−4] Since synthetic plastics are extremely resistant to natural degradation, most plastic wastes that are either discarded into landfills or mishandled will remain in those environments for decades to centuries.[5−7] Therefore, interventions are required to recycle the plastic waste or break down the polymeric chains into significantly shorter fragments, e.g., gaseous or liquid products, instead of microplastics[8] (≤5 mm) or nanoplastics[8] (≤1 μm).

While mechanical recycling remains the most prevalent way of recycling solid plastic waste,[9,10] it is typically limited to high-purity plastic waste, since the presence of contaminants and additives within the waste mixture will degrade the final quality of the recycled products.[11,12] More recently, thermochemical recycling has been touted as a prospective solution that can address certain shortcomings of mechanical recycling,[10] while still providing environmental advantages over landfilling and incineration.[13−15] Regardless of the thermochemical recycling technology (e.g., gasification or pyrolysis), the utilization of catalysts within these processes lowers the reaction temper-

Received: February 26, 2024
Revised: April 18, 2024
Accepted: April 18, 2024

© XXXX American Chemical Society

https://doi.org/10.1021/acscatal.4c01213
ACS Catal. 2024, 14, 7536−7552

ature required to attain a similar degree of polymer deconstruction or product yields.[16−20] Furthermore, catalysts, particularly ones with size-and-shape selectivity, i.e., zeolites, can also enable fine-tuning of the final product distribution and allow for higher selectivity to desired, high-value products.

A variety of hydrocarbon conversions rely on zeolites, since their microporous channels and voids impose confinement effects on guest species via van der Waals interactions, thereby altering reactivity and selectivity.[21−26] These interactions can stabilize the carbenium/carbonium ion transition states that govern hydrocarbon reactions, including beta scission,[23,27] which proceeds via a carbenium ion pathway and is typically the main Brønsted acid-catalyzed reaction responsible for the deconstruction of long-chain polymers or shorter-chain alkenes into smaller fragments at milder temperatures (<673 K). However, the microporosity of zeolites also restricts the diffusion of bulky molecules into internal active Brønsted acid sites (BAS),[28−31] leading to lower overall catalyst efficiency. One common approach to alleviate diffusion limitations for microporous materials is to introduce a new level of porosity (e.g., mesoporosity or macroporosity) to yield hierarchical zeolites.[32−34]

While bifunctional metal+acid (zeolite) catalysts are employed in traditional hydrocracking of polyolefins,[35−39] metal-free zeolites have also been shown to facilitate scission of polyolefins.[40 −43] Furthermore, within the context of medium pore zeolites, i.e., MFI, metal-free hierarchical MFI zeolites have been reported as more active from higher conversion or lower degradation temperature via thermogravimetric analysis (TGA) than their purely microporous counterparts for polyolefin deconstruction over a broad range of reaction temperatures and conditions (flow/thermogravimetric and batch).[44−50] These observations are proposed to be due to easier ingress of bulky molecules, i.e., higher accessibility to acid sites,[44,46−48,50] and higher external surface areas that allow for greater contact between the melted polymer and catalyst surface due to mesopore formation.[44,46] Additionally, the enhanced accessibility of BAS within hierarchical zeolites can be systematically quantified and compared with parent zeolites via an accessibility factor,[49−51] which is defined as the ratio of BAS detected by a bulkier alkylpyridine molecule (e.g., 2,4,6-trimethylpyridine) to pyridine. Indeed, the accessibility factors of hierarchical MFI are generally higher than parent MFI, regardless of the synthetic methods used.[49−51] The benefits of introducing a secondary level of porosity are not restricted to medium pore MFI zeolites, since hierarchical FAU zeolites synthesized via desilication have also been shown to fully degrade polyethylene at lower temperatures than parent FAU zeolites.[52,53]

Although the benefits of mesopore incorporation within MFI and FAU zeolites are well reported in the literature, the impacts of mesopore connectivity (open or constricted mesopores) and mesopore type (mesopores within microporous framework or composites of zeolite/ordered mesoporous materials (OMM)) on plastic deconstruction rates (normalized by density of BAS), product selectivities, and catalyst recyclability at milder reaction temperatures, remain largely unknown. Herein, we report on the synthesis of hierarchical MFI (10-membered ring (MR)) and FAU (12-MR) catalysts under varying desilication conditions (e.g., temperature, time, with or without surfactants), and the performance of solvent-free polyethylene (PE) catalytic cracking reactions under mild reaction conditions (473 K, 10 bar initial H_2) in investigations of how the incorporation of mesopores with varying pore connectivities into conventionally microporous zeolite framework augment solid conversion rates and desired product selectivities. Additionally, isothermal TGA in an inert Ar environment was performed on physical mixtures of PE + zeolites to both monitor the rate of PE deconstruction as a function of time and compare trends of solid conversion rates with those from batch reactions in an H_2 environment. Results from batch and TGA experiments unequivocally show that the incorporation of mesopores within MFI increases solid conversion rates, but not on FAU, presumably because the hierarchical FAU materials synthesized via desilication with cetyltrimethylammonium bromide (CTABr) are composites of hierarchical FAU and ordered mesoporous materials, rendering weaker confinement effects. Recyclability experiments were also performed on parent and hierarchical MFI and FAU catalysts to elucidate how the presence of mesopores within different zeolite frameworks affects catalyst stability and deactivation. Collectively, the results herein provide important insights into the impact of different mesopore incorporation strategies within microporous zeolites for deconstruction of plastic waste into shorter-chain hydrocarbons.

2. EXPERIMENTAL METHODS

2.1. Catalyst Synthesis. Hierarchical MFI zeolites (H-MFI-hier*Y*; *Y* = desilication treatment time in minutes) without surfactants were synthesized via postsynthetic desilication by following procedures previously published.[54−56] A commercial MFI zeolite (Si/Al ratio = 40; Zeolyst, CBV 8014) in the NH_4^+ form was calcined at 823 K (2 K min^{-1}) for 8 h under dry air flow (Airgas, Zero grade, 75 cm^3 min^{-1} (g solids)$^{-1}$) to yield MFI in the protonated form (H-MFI) for subsequent desilication. Briefly, a 0.2 M NaOH solution (Fisher Scientific, 98.7%, 30.3 cm^3 g^{-1}) was added to a 500 mL HDPE bottle and suspended in an oil bath at either 333 K (H-MFI-hierY-333 K) or 338 K (H-MFI-hierY-338 K) for 30 min. Parent H-MFI-40 (4 g; nominal Si/Al ratio = 40) was then added to the heated NaOH solution while stirring for different time periods (*Y* = 15, 30, or 60 min) and subsequently quenched with ice water for 20 min after the desired time was reached. The samples were then recovered via centrifugation and cyclically washed with deionized (DI) water (18.2 MΩ·cm) until the supernatant reached pH ≤ 9. These samples were then dried in a convection oven (Yamato, DKN402C) at 353 K overnight to produce hierarchical MFI samples in the Na^+-form. The hierarchical MFI samples were ion-exchanged three times (2 h each) with aqueous NH_4NO_3 (≥0.5 M, Fisher Scientific, 99.8%, 100 cm^3 g^{-1}) at 353 K, recovered via vacuum filtration, and rinsed with DI water (≥500 mL) before drying at 353 K overnight in an oven. The NH_4^+-hierarchical zeolites were calcined at 823 K (2 K min^{-1}) for 8 h under continuous air flow to yield hierarchical zeolites in the protonated form.

Hierarchical MFI zeolite desilicated in the presence of tetrapropylammonium bromide (TPABr; Sigma-Aldrich, 98%) as a surfactant was prepared following a similar procedure described above, with the exception that (i) 0.2 M of TPABr was present in the NaOH solution prior to addition of the parent H-MFI zeolite and (ii) the washed and dried desilicated sample was calcined at 823 K (2 K min^{-}) for 8 h to remove surfactants prior to NH_4^+-ion exchange. The desilication procedure was performed at 338 K for 30 min.The hierarchical MFI zeolite synthesized with TPABr is denoted as H-MFI-hier30-338 K-TPA.

https://doi.org/10.1021/acscatal.4c01213
ACS Catal. 2024, 14, 7536−7552

Commercial parent H-FAU-15 (nominal Si/Al ratio = 15; Zeolyst, CBV 720) and H-FAU-40 (nominal Si/Al ratio = 40; Zeolyst, CBV 780) were ion-exchanged three times (2 h each) with aqueous NH_4NO_3 (≥0.5 M, 100 cm^3 g^{-1}) at 353 K to remove synthetic residues. The parent NH_4^+-FAU zeolites were then converted to the H^+-form following an identical procedure described above (washing, drying, and calcination) before performing plastic upcycling reactions.

Hierarchical FAU zeolites were synthesized via desilication with cetyltrimethylammonium bromide (CTABr; Sigma-Aldrich, ≥ 96%) as a surfactant. Commercial H-FAU zeolites were utilized as received, with no prior ion-exchange with NH_4^+, for subsequent desilication. The desilication procedure was similar to that described above for desilication of MFI zeolites with surfactants, but 0.2 M CTABr was used instead of TPABr. The parent and hierarchical FAU zeolites are denoted as H-FAU-X and H-FAU-X-CTA, respectively, where X = Si/Al ratio of parent zeolites.

2.2. Catalyst Characterization. Crystallinity of hierarchical MFI and FAU materials was determined via powder X-ray diffraction with a diffractometer (Bruker, D8 Discover, Cu Kα radiation) under ambient conditions (scan rate = 5° min^{-1}). Small-angle X-ray scattering (SAXS) experiments were performed with an X-ray scattering system (Xenocs, Xeuss 3.0) equipped with a beam delivery system (Xenocs, GeniX 3D) that produces a high intensity, monochromatic Cu Kα beam. The samples were loaded onto a 15-slot powder sample holder (Xenocs) and held in place with Kapton windows (12.5 μm thick) and O-rings. The Si/Al ratios of parent and hierarchical materials were determined by energy dispersive X-ray analysis in a scanning electron microscope (EDX-SEM; Quanta, 200). The samples were loaded onto carbon tape attached to a flat SEM specimen stub and subsequently loaded into the SEM for analysis. The analysis was performed at 10 kV, $<5 \times 10^{-5}$ Torr, a working distance of 10 mm, and a scan time of 5 min for each selected area of analysis. Transmission micrographs of the samples were collected with a transmission electron microscope (TEM; Talos, F200X) at 200 kV.

Density of BAS was determined via n-propylamine temperature-programmed desorption with a thermogravimetric analyzer (NPA-TGA). TPD of alkylamines has been utilized extensively to reliably determine the density of BAS of microporous aluminosilicates.[57−60] Here, NPA-TGA was benchmarked first with a thermogravimetric analyzer (PerkinElmer, TGA8000) connected to a mass spectrometer (PerkinElmer, Clarus SQ8T) with heated transfer lines (533 K) at the Princeton Imaging and Analysis Center (IAC). These experiments determined the weight loss region that corresponds to the Hoffmann elimination reaction of NPA to form propene (and ammonia), instead of NPA desorption. NPA (Sigma-Aldrich, ≥99%) was dosed onto the sample ex situ by adding 150 μL of NPA to 50 mg of sample in a scintillation vial. The scintillation vial was left uncovered in a fume hood overnight (>12 h) to allow for evaporation of liquid NPA under ambient conditions. The dried sample was loaded onto a ceramic pan, and the temperature was ramped from 303 to 423 K (10 K min^{-1}; 2 h hold) under He flow (25 cm^3 min^{-1} sample flow, 50 cm^3 min^{-1} purge flow) to remove residual water and NPA; subsequently, the temperature was ramped to 673 K (10 K min^{-1}; 30 min hold). Figure S1 shows that propene elutes at t > 150 min (T = 673 K) for both H-MFI-40 and H-MFI-hier30−338 K. Thus, the weight loss from 150 to 200 min was taken as the weight loss of NPA that undergoes the Hoffmann elimination reaction and used to determine the moles of BAS. NPA-TGA experiments were then carried out without MS on a different thermogravimetric analyzer (PerkinElmer, TGA8000) following a similar procedure (Figure S2) under Ar flow (30 cm^3 min^{-1} sample flow, 60 cm^3 min^{-1} purge flow). The density of BAS of H-MFI-40 and H-MFI-hier30−338 K determined from both set ups are similar (≤0.03 mmol BAS g^{-1}). The BAS densities reported here are from TGA experiments performed without MS.

Densities of weak and strong acid sites were also characterized by NH_3-TPD with a chemisorption analyzer (Micromeritics, AutoChem II). The desorption peaks at low (373−523 K) and high (523−873 K) temperatures (Figure S3) were assigned to weak and strong acid sites, respectively. Catalysts were first pretreated *in situ* at 673 K (10 K min^{-1}) under continuous He flow (Airgas, Ultrahigh purity grade, 30 cm^3 min^{-1}) for 1 h to remove adsorbed H_2O. The catalysts were then cooled to 373 K, and the gas flow was switched to 10% NH_3 (balance He; Airgas, 30 cm^3 min^{-1}). The samples were held at 373 K for 2 h to allow for adsorption of NH_3, and the gas flow was switched back to He (30 cm^3 min^{-1}) for 1 h to desorb weakly adsorbed NH_3. The sample was then ramped from 373 to 973 K (10 K min^{-1}) under He flow (30 cm^3 min^{-1}), and the amount of NH_3 desorbed was monitored with a thermal conductivity detector.

Diffuse reflectance infrared Fourier transform spectroscopy (DRIFTS) of acetonitrile-d_3 (CD_3CN; Sigma-Aldrich, ≥99.8% atom D) was used to determine the ratio of Lewis to Brønsted acid sites on parent and hierarchical samples. The spectra were collected with a spectrometer (Bruker, INVENIO) with a liquid N_2 cooled HgCdTe detector. The catalyst sample (20−30 mg) was loaded into a high-temperature reaction chamber (Harrick, Praying Mantis) that is attached to a diffusion reflectance accessory (Harrick, Praying Mantis) and dehydrated at 673 K (10 K min^{-1}) for 30 min under vacuum (~2 torr) with N_2 flow (20 cm^3 min^{-1}). The sample was then cooled from 673 to 303 K, and CD_3CN (~1 μL per dose) was dosed into the reaction chamber via a syringe injection port connected to the inlet line. DRIFTS spectra were collected after each dose, and the dosing was stopped after no further change in the targeted bands was observed. The final DRIFTS spectra (128 scans, 4 cm^{-1} resolution) were obtained after physisorbed CD_3CN fully desorbs from the samples (~15 min).

Physical properties, e.g., pore volume, surface areas, and pore-size distribution, of the synthesized materials were characterized by N_2 physisorption at 77 K with an adsorption analyzer (Micromeritics, 3Flex). The samples were degassed overnight at 393 K under reduced pressure (125 Torr) with a Schlenk line before the samples were loaded into the adsorption analyzer. The micropore volume (V_{micro}), micropore surface area (S_{micro}), and external surface area ($S_{external}$) of each sample were obtained from the t-plot method using the Harkins−Jura model. The mesopore volume (V_{meso}) and mesopore surface area (S_{meso}) were obtained from the Barrett−Joyner−Halenda (BJH) adsorption curves (Faas correction, 2−50 nm).

2.3. Batch PE Catalytic Cracking Experiments. Batch catalytic cracking of PE in an H_2 environment was carried out in a stainless-steel reactor (Parr Instrument, 450 mL, Series 4567) equipped with a pressure transducer (Dwyer, Series 626). Commercial PE (Sigma-Aldrich, 4000 Da) and a catalyst sample, at a 5:1 PE-to-catalyst mass ratio, were ground and

https://doi.org/10.1021/acscatal.4c01213
ACS Catal. 2024, 14, 7536−7552

mixed together with a mortar and pestle before the mixture was added to the reactor vessel. The reactor containing the catalyst mixture was sealed and purged with a continuous N_2 flow (Airgas, Ultrahigh purity grade) for 5 min, then charged and purged five times with H_2 (Airgas, Ultrahigh purity grade). After the final purge, the reactor was charged to the desired reaction pressure. The reactor was then heated to the specified temperature with a commercial cylindrical heater (Parr Instrument, A2230HC2EB) connected to a temperature controller (Omega, CND3). The thermocouple (Parr Instrument, type K) used for temperature control is located within the reactor and situated slightly above the solid mixture (~1−2 cm). After the designated reaction time, the cylindrical heater was removed, and the sealed reactor was cooled in an ice bath for 15 min to a temperature below 283 K. The gas in the reactor headspace was then collected in a gas bag and analyzed via GC-FID (Thermo Scientific, Trace 1300). The partial pressures of gaseous products were determined by using response factors of pure alkane gases (C_1−C_3) and direct injection of a C_1−C_6 standard gas mixture (Airgas; 83.2 mol % H_2, 5.004 mol % CH_4, 5.020 mol % C_2H_6, 5.017 mol % C_3H_8, 1.002 mol % C_4H_{10}, 0.5026 mol % C_5H_{12}, 0.2520 mol % C_6H_{14}), and the gaseous yields were determined with ideal gas law based on the final reactor pressure. The gaseous product selectivity is determined by taking the ratio of the specific gaseous product range (e.g., C_2−C_3) to the total amount of gaseous products produced. The liquid products were recovered with 10 mL of dichloromethane (DCM) and analyzed by GC-FID (Agilent, 7890A) and ^{1}H NMR (Bruker, 500 MHz). For liquid product analysis via GC-FID, mesitylene (1.5 μL) was added to 5 mL of the recovered liquid solution as an internal standard. For liquid product analysis via ^{1}H NMR, 45 μL of the recovered liquid solution was added to 555 μL of $CDCl_3$ (Sigma-Aldrich, 99.8% atom D). The solid residue within the reactor was recovered with acetone and transferred to a preweighed beaker. The acetone was evaporated from the beaker at 323 K for >4 h, and the mass of the solid residue was utilized to determine solid conversion:

$$\text{Solid conversion}(\%) = \frac{m_{\text{PE}} + m_{\text{catalyst}} - m_{\text{solid residue}}}{m_{\text{PE}}} \times 100\% \quad (1)$$

where m_{PE} and m_{catalyst} are the initial mass of the loaded PE and catalyst, respectively, and $m_{\text{solid residue}}$ is the mass of solid residue after reaction. A detailed schematic of the reactor configuration and further details of product characterization and quantification are provided in our earlier study.[40]

2.4. Thermogravimetric Analysis on Physical Mixtures of PE and Catalyst. Reactions of physical mixtures of commercial PE and catalyst were analyzed on a thermogravimetric analyzer (PerkinElmer, TGA8000) to track the mass loss of PE with respect to time and obtain solid conversion rates. First, 200 mg of PE and 40 mg of catalyst were gently ground and mixed with a mortar and pestle and approximately 10 mg of this mixture was then loaded onto a ceramic pan. The thermogravimetric experiment was carried out under an inert Ar flow (Airgas, Ultrahigh purity grade, 30 cm^3 min^{-1}), and the sample was first heated from 303 to 423 K (10 K min^{-1}; 2 h hold) to remove H_2O from the sample. The sample temperature was then ramped to 523 K (10 K min^{-1}) and held there for 5 h to emulate PE catalytic cracking in a batch reaction (Section 2.3). After 5 h, the sample was ramped to 873 K (10 K min^{-1}) to deconstruct the remaining PE. The gas flow was switched from Ar to air (Airgas, Zero grade, 30 cm^3 min^{-1}) to burn off coke deposits on the catalyst for 20 min at 873 K, and the final mass after this isothermal hold was used as the mass of initial catalyst loaded onto the pan. The thermogravimetric analyzer was calibrated for temperature accuracy using alumel, nickel, perkalloy, and iron supplied by PerkinElmer to obtain the apparent Curie transitions (Table S1). The reproducibility of solid conversion rates obtained from isothermal thermogravimetric experiments was also confirmed by repeating the experiments three times using H-MFI-hier30−338 K and H-MFI-hier30−338 K-TPABr (Figures S4 and S5).

Recyclability of the suite of catalysts was also probed through TGA but with a slightly different procedure. For the first cycle, approximately 5 mg of the catalyst was directly loaded onto a ceramic pan followed by 5 mg of PE. The PE-catalyst mixture was first heated from 303 to 423 K under Ar flow (10 K min^{-1}; 1 h hold) to remove H_2O from the zeolites. The mixture was then ramped from 423 to 573 K (10 K min^{-1}; 1 h hold) for PE deconstruction, and subsequently cooled back down to room temperature. For the second cycle, roughly 5 mg of PE was loaded onto the pan with the spent catalysts, and the TGA experiment was initiated following the identical procedure as that for the first cycle. The procedure for the third cycle resembles that for the second cycle, but Ar gas was switched to air after the 1 h hold at 573 K and followed by a temperature ramp from 573 to 1023 K to determine the amount of coke accumulated on the catalyst after three recyclability cycles.

2.5. *In situ* ^{13}C and ^{1}H MAS NMR. In situ ^{1}H and ^{13}C MAS NMR experiments were carried out using a Varian Inova wide-bore 300 MHz NMR spectrometer equipped with a 7.5 mm commercial Vespel MAS NMR probe and a commercial heating stack for variable temperature experiments. The corresponding Larmor frequencies for ^{1}H and ^{13}C were 299.97 and 75.43 MHz, respectively. Zeolite samples were dehydrated at 723 K for 5 h under He (50 mL/min) in an airtight reactor and subsequently transferred to a glovebox purged by N_2. The zeolites and PE (Sigma-Aldrich, 4000 Da) samples were packed within the glovebox into a sealed MAS NMR rotor[61−63] with a net sample volume space of 300 μL that is capable of high temperature and high pressure NMR studies. Both the single pulse (SP) ^{13}C and ^{1}H MAS NMR experiments used a sample spinning rate of 4 kHz. The SP experiments were acquired with a 45-degree angle pulse with a pulse width of 2 μs and a recycle delay of 20 s with an accumulation number variable between 128 and 2000 depending on the type of experiments, either ^{1}H or ^{13}C. All the spectra were referenced to TMS (0 ppm) and by using adamantane as a second reference (38.48 ppm for its downfield ^{13}C peak and 1.82 ppm for the center band of ^{1}H).

3. RESULTS AND DISCUSSION

3.1. Assessing Crystallinity, Mesopore Volume and Connectivity, and Acid Site Density of Hierarchical MFI and FAU Zeolites. The hierarchical MFI and FAU zeolites synthesized via desilication at different reaction conditions provided a suite of MFI and FAU samples with differing pore connectivities and diameters from their parent counterparts (H-MFI-X and H-FAU-X; X = Si/Al ratio). Specifically, H-MFI-hier*Y* (*Y* = desilication time in minutes; 15, 30, or 60 min) catalysts were synthesized at two different desilication

https://doi.org/10.1021/acscatal.4c01213
ACS Catal. 2024, 14, 7536−7552

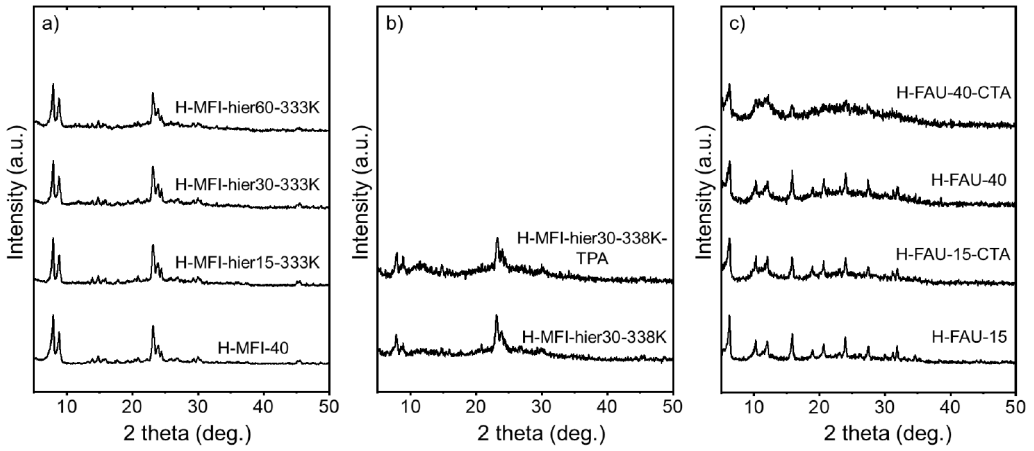

Figure 1. X-ray diffractograms of (a,b) parent and hierarchical MFI synthesized under different reaction conditions (reaction time, desilication temperatures, with or without surfactants) and (c) parent and hierarchical FAU catalysts. The diffractograms are vertically offset for clarity.

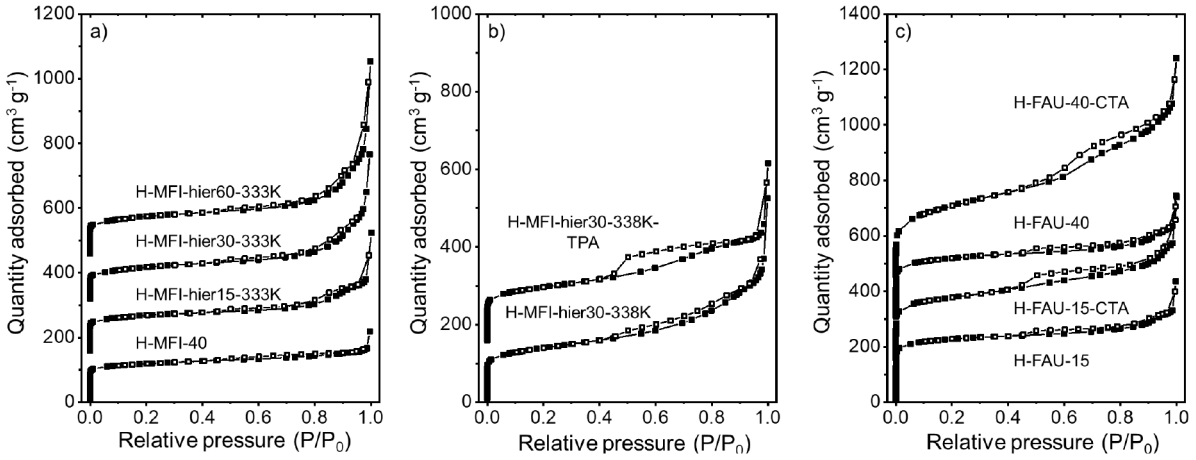

Figure 2. N_2 physisorption isotherms of (a) parent H-MFI-40 and H-MFI-hierX-333 K, (b) H-MFI-hier30−338 K and H-MFI-hier30−338 K-TPA, and (c) parent and hierarchical FAU materials. The physisorption isotherms are vertically offset by +125 $cm^3\ g^{-1}$ for clarity.

temperatures (333 or 338 K) either with or without the TPABr surfactant. The presence of TPA^+ during the desilication treatment was previously shown to form constricted rather than open mesopores, because the TPA^+ cations can interact strongly with the catalyst surface and partially preserve the microporosity of the catalyst surface.[56] Hierarchical FAU zeolites (H-FAU-X-CTA; X = Si/Al ratio of parent FAU) were synthesized under the same reaction conditions (338 K, 30 min desilication, CTABr surfactant) with either H-FAU-15 or H-FAU-40 as the parent zeolite. The presence of a surfactant is necessary for desilication of H-FAU samples with high (>4) Si/Al ratios, because the crystallinity and microporosity of the FAU framework are not preserved otherwise.[52,64] Additionally, CTABr was chosen as the surfactant for desilication of H-FAU because the presence of CTA^+ has been reported to concurrently form ordered mesoporous materials from the dissolved siliceous species on the external surface of FAU while forming intracrystalline mesopores (due to the presence of NaOH).[65] Therefore, H-FAU-15-CTA and H-FAU-40-CTA are likely zeolite/OMM composites, where the high surface area and mesoporous nature of OMMs can enable both enhanced diffusion to active sites and polymer-catalyst interactions.

X-ray diffractograms of H-MFI-hierX-333 K resemble that of parent H-MFI-40 (Figure 1a), which shows that the desilication treatment at 333 K did not drastically affect the crystallinity of the zeolites. At a slightly higher desilication temperature of 338 K, the crystallinities of the MFI framework are slightly reduced (Figure 1b), as demonstrated by the reduced intensity of the diffraction peaks at 2θ = 9° and 23°. Nonetheless, the diffractograms still contain crystallographic features that are characteristic of the MFI framework. As shown in Figure 1c, the diffraction peaks of H-FAU-15-CTA are similar to H-FAU-15, but those of H-FAU-40-CTA are less prominent than for H-FAU-40. The more significant loss in crystallinity for H-FAU-40-CTA is due to the higher initial Si/Al ratio of the parent H-FAU-40 used for desilication, because a sufficient density of framework Al atoms (and thus, AlO_4^-) was previously shown to protect against extensive dissolution of Si−O−Si bonds.[66]

Figure 2 shows N_2 physisorption isotherms of the suite of synthesized MFI and FAU materials. The textural properties obtained from these isotherms are tabulated in Tables 1 and S2. In general, all of these hierarchical zeolites exhibited a combined type I−IV isotherm that is characteristic of mesopore formation after desilication of microporous zeolites.[67] Additionally, the adsorption and desorption branches of zeolites desilicated in the absence of surfactants are parallel to each other, which suggests formation of open mesopores that are connected to the zeolite surface (Figure

https://doi.org/10.1021/acscatal.4c01213
ACS Catal. 2024, 14, 7536−7552

Table 1. Textural Properties of Parent and Hierarchical MFI and FAU Catalysts

catalyst	V_{micro} [a] ($cm^3\ g^{-1}$)	V_{meso} [b] ($cm^3\ g^{-1}$)	S_{micro} [a] ($m^2\ g^{-1}$)	S_{meso} [b] ($m^2\ g^{-1}$)
H-MFI-40	0.13	0.09	280	75
H-MFI-hier15−333 K	0.12	0.20	231	86
H-MFI-hier30−333 K	0.10	0.41	205	120
H-MFI-hier60−333 K	0.10	0.47	231	110
H-MFI-hier30−338 K	0.11	0.41	220	258
H-MFI-hier30−338 K-TPA	0.12	0.36	260	290
H-FAU-15	0.26	0.18	560	97
H-FAU-15-CTA	0.21	0.40	430	310
H-FAU-40	0.23	0.20	480	110
H-FAU-40-CTA	0.11	0.77	250	610

[a]Determined by the t-plot method. [b]Determined from BJH adsorption isotherm.

2a,b). In contrast, when desilication was performed in the presence of a surfactant (TPABr or CTABr), a flatter desorption branch followed by a sharp decrease at lower relative pressures was observed (Figure 2b,c). The resulting, more pronounced, hysteresis loops on H-MFI-hier30−338 K-TPA, H-FAU-15-CTA, and H-FAU-40-CTA indicate that the mesopores formed on these materials are more constricted (accessible through larger entrances that are <4 nm in diameter) or occluded (only accessible through micropores)[56] instead of fully open to the crystal surface. The physisorption isotherm of H-FAU-40-CTA also displayed more significant N_2 uptake across P/P_0 in the range of 0.2−1.0 compared to other H-FAU samples (Figure 2c), which indicates formation of larger amounts of OMM.

Increasing the desilication time from 15 to 60 min on H-MFI-hierY-333 K increases mesopore volume from 0.20 to 0.47 $cm^3\ g^{-1}$ without a significant decrease in micropore volume (<0.02 $cm^3\ g^{-1}$; Table 1). Additionally, the center of the pore size distribution of mesopores (d_p) increases from 8.7 to 12.6 nm, with a concomitant increase in the full width at half-maximum (fwhm) of the distribution curve (Figure S6). The micropore and mesopore volumes of H-MFI-hier30−338 K and H-MFI-hier30−338 K-TPA are similar (ΔV_{micro} <0.01 $cm^3\ g^{-1}$ and ΔV_{meso} <0.05 $cm^3\ g^{-1}$; Table 1), but the d_p and pore size distribution of H-MFI-hier30−338 K-TPA are, respectively, smaller (d_p = 3.7 nm) and narrower than that of H-MFI-hier30−338 K (d_p = 5.2 nm; Figure S6). Furthermore, TEM images (Figure 3) show that H-MFI-hier30−338 K has mesopores that are connected to the crystal surface, while H-MFI-hier30−338 K-TPA has mesopores that are more constricted/occluded and a more-preserved crystal surface. These results are consistent with those reported from a prior study from which the synthesis procedure herein was adapted,[56] where extensive characterization using multiple techniques (positron annihilation lifetime spectroscopy, scanning transmission electron microscopy, N_2 physisorption, and mercury porosimetry) was performed to verify the pore network (constricted/occluded or open) of hierarchical MFI zeolites synthesized with or without TPABr as surfactant. Importantly, within the same study,[56] N_2 physisorption experiments on hierarchical MFI zeolite synthesized with TPABr showed identical N_2 uptake at P/P_0 > 0.2 before and after saturation with *n*-nonane that plugs micropores, which strongly indicates that the vast majority of intracrystalline mesopores are constricted instead of occluded mesopores. Therefore, we presume that the H-MFI-hier30−338 K-TPABr synthesized in this study by following the identical procedure[56] also yields mainly constricted instead of occluded mesopores.

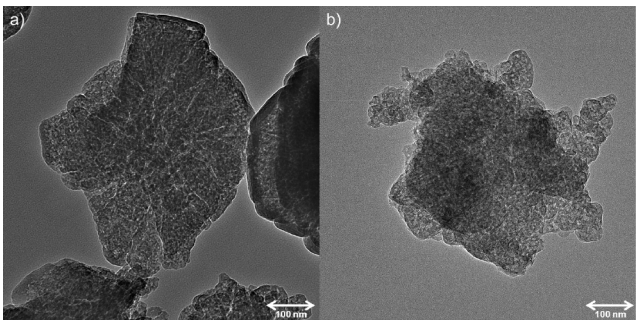

Figure 3. TEM images of (a) H-MFI-hier30−338 K and (b) H-MFI-hier30−338 K-TPA.

Similar to hierarchical MFI catalysts, the mesopore volumes of hierarchical FAU zeolites are greater than their parent counterparts, but with a slightly more significant decrease in micropore volume compared to MFI (Table 1). The commercial parent FAU zeolites (H-FAU-15 and H-FAU-40) contain non-negligible amounts of mesopores in the framework (Table 1), due to the steam and acid treatments needed to attain higher Si/Al ratios (>2) on FAU-type, i.e., USY, materials. However, the mesopores formed via steam and dealumination on FAU are typically occluded and present as cavities, and therefore, do not drastically impact intracrystalline diffusion.[68,69] Hence, although parent FAU zeolites utilized here are technically hierarchical in nature, the desilication treatment performed in the presence of CTABr further increases mesopore volumes (+122% on H-FAU-15-CTA and +285% on H-FAU-40-CTA; Table 1 and Figure S6), which indicates an increase in the amount of both interconnected mesopores and mesopores originating from OMM. The ratio of OMM to interconnected mesopores is likely higher on H-FAU-40-CTA than H-FAU-15-CTA, since the distribution of mesopores formed on H-FAU-40-CTA is more concentrated around the 3−5 nm region (Figure S6). The higher amount of OMM formed is likely due to more extensive leaching of Si and Al species from the parent H-FAU-40 catalyst (Figure 1), which can facilitate recrystallization.

SAXS was performed on H-FAU materials to obtain additional structural information on the zeolite/OMM composites and for comparison with commercial Al-MCM-41 (Figure 4). The feature at q = 4.5 nm^{-1} is characteristic of the FAU framework and is present in all these H-FAU materials, consistent with our XRD results. This feature, as expected, is absent in commercial Al-MCM-41. The SAXS pattern for Al-MCM-41 contains features centered around q = 1.4 nm^{-1} and 2.8 nm^{-1} that are characteristic of the periodic ordering of mesostructures within Al-MCM-41,[70] but these features are absent for H-FAU-15-CTA and H-FAU-40-CTA. This indicates that the periodicity of the mesostructures formed on the hierarchical H-FAU materials is much shorter in range than that for Al-MCM-41, because the mesostructures coexist with the microporous structure of parent H-FAU that cannot be fully dissolved under mild desilication conditions (338 K, 30 min).

https://doi.org/10.1021/acscatal.4c01213
ACS Catal. 2024, 14, 7536−7552

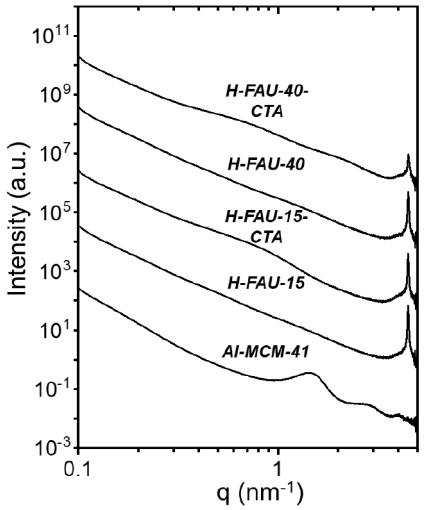

Figure 4. SAXS pattern of commercial Al-MCM-41 and parent and hierarchical FAU materials. The SAXS curves are vertically offset by ×100 for clarity.

EDX-SEM, NPA-TGA, and NH_3-TPD were used to determine the Si/Al ratios, BAS density, and weak and strong acid site densities, respectively, of the parent and hierarchical MFI and FAU catalysts (Table 2). We note that the density of strong acid sites of H-MFI-40 determined from NH_3-TPD (0.35 mmol g^{-1}) is similar to the density of BAS determined from NPA-TGA (0.36 mmol g^{-1}), and both values agree with BAS densities reported in literature on identical commercial H-MFI-40 (Zeolyst, CBV 8014) via iso-propylamine-TPD[58] or pyridine-IR[71] (0.33−0.34 mmol g^{-1} BAS). In general, the Si/Al ratios of the hierarchical MFI (Si/Al = 28−39) and FAU zeolites (Si/Al = 16 and 30 on H-FAU-15-CTA and H-FAU-40-CTA, respectively) are lower than that of the respective parent zeolites (Si/Al = 41 on H-MFI-40, Si/Al = 17 on H-FAU-15, and Si/Al = 66 on H-FAU-40). This decrease in Si/Al ratio manifests in higher density of BAS on all hierarchical samples and higher density of strong acid sites on hierarchical FAU, compared to their parent counterparts. The densities of strong acid sites on hierarchical MFI, however, are similar to parent MFI (≤0.06 cm^3 g^{-1}; Table 2). Since desilication changes the micropore and mesopore volumes of MFI, and thus, decreases confinement effect, some of the NH_3 molecules can potentially desorb at lower temperatures that are typically associated with weak acid sites, leading to underestimation of BAS density with NH_3-TPD. This difference, however, does not affect the trend of solid conversion rates, as the trend remains similar regardless of whether solid conversion is normalized by BAS or strong acid sites (Section 3.2; *vide infra*). Further, this indicates that BAS are mostly preserved after desilication treatment under the mild conditions used here (0.2 M NaOH, 338 K, 0.5 h).

Taken together, results from this section show that desilication treatments on parent H-MFI and H-FAU performed across different reaction conditions, e.g., several temperatures, reaction times, and with or without surfactant, successfully incorporate mesopores into the predominantly microporous structure while not decreasing the density of strong/Brønsted acid sites significantly. The different reaction conditions utilized for desilication yielded a suite of samples with varying mesopore volumes and connectivities, enabling investigations of the impact of these mesoporous architectures on PE conversion reactions, as will be discussed in subsequent sections.

3.2. Effects of Hierarchical MFI and FAU Pore Architectures on Solid Conversion Rate and Product Selectivity. Batch PE degradation reactions were performed to elucidate the impact of different pore diameters and connectivities within hierarchical zeolites for plastic upcycling applications. Figure 5a shows that both the solid conversion amount and the solid conversion rate gradually increase from 14 to 26% and 380 to 540 $\frac{g\text{PEconsumed}}{\text{molBAS}\cdot h}$, respectively, on MFI with longer desilication times (from 0 to 30 min), which is correlated with the increase in mesopore volumes of +0.32 cm^3 g^{-1} (Table 1). The solid conversion amount and solid conversion rate plateau with further increases in MFI desilication time (from 30 to 60 min), which is consistent with similar resultant mesopore volumes (Δ < 0.06 cm^3 g^{-1}; Table 1) and pore size distributions (d_p = 12.6 nm; Figure S6). The trend in solid conversion rate does not change significantly regardless of whether Brønsted or strong acid sites were used to normalize solid conversion (Figure S7), due to relatively small difference between the density of Brønsted and strong acid sites (Table 2).

Interestingly, the solid conversion (39%) and solid conversion rate (810 $\frac{g\text{PEconsumed}}{\text{molBAS}\cdot h}$) on H-MFI-hier30−338 K with open mesopores are slightly lower than those on H-MFI-hier30−338 K-TPA (43% and 932 $\frac{g\text{PEconsumed}}{\text{molBAS}\cdot h}$) with constricted mesopores. This indicates that increases in solid conversion rate are not solely dependent on the accessibility of parent PE chain to acid sites within the micropores of MFI,

Table 2. Si/Al Ratio and Density of Acid Sites of Parent and Hierarchical Catalysts

catalyst	density of *weak* acid sites[a] (mmol g^{-1})	density of *strong* acid sites[a] (mmol g^{-1})	density of BAS[b] (mmol g^{-1})	Si/Al[c]
H-MFI-40	0.29	0.35	0.36	41
H-MFI-hier15−333 K	0.32	0.30	0.40	39
H-MFI-hier30−333 K	0.34	0.29	0.47	30
H-MFI-hier60−333 K	0.35	0.35	0.49	28
H-MFI-hier30−338 K	0.34	0.33	0.48	28
H-MFI-hier30−338 K-TPA	0.32	0.39	0.46	32
H-FAU-15	0.15	0.49	0.60	17
H-FAU-15-CTA	0.22	0.56	0.71	16
H-FAU-40	0.05	0.12	0.21	66
H-FAU-40-CTA	0.06	0.26	0.34	30

[a]Determined via NH_3-TPD. [b]Determined via NPA-TGA. [c]Determined via EDX-SEM.

https://doi.org/10.1021/acscatal.4c01213
ACS Catal. 2024, 14, 7536−7552

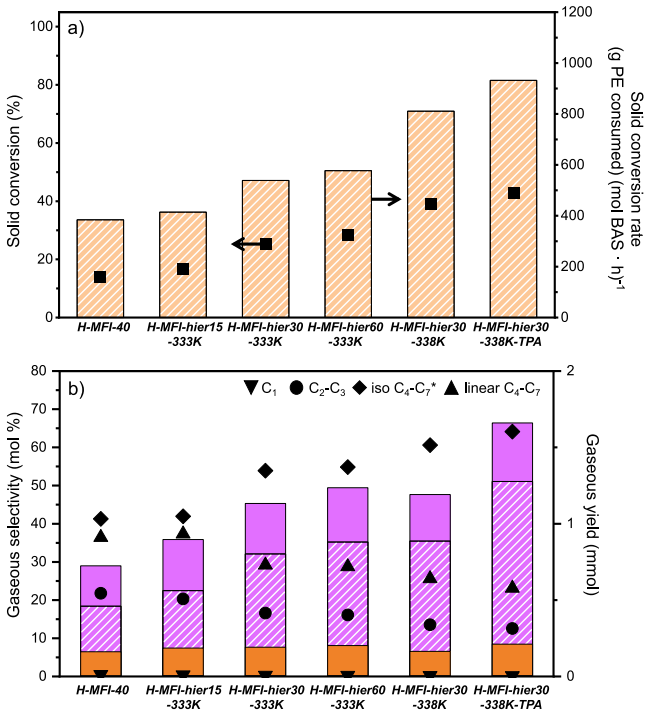

Figure 5. (a) Solid conversion (■) and solid conversion rate (striped bars) for PE catalytic cracking on parent and hierarchical MFI catalysts. (b) Gaseous product selectivity and yield for PE catalytic cracking on parent and hierarchical MFI catalysts. Orange and purple solid bars indicate C_2-C_3 and C_4-C_7 linear alkanes, respectively, while orange and purple striped bars indicate C_1 and C_4-C_7 isoalkanes, respectively. *indicates that C_4-C_7 alkenes are also present and included in this value. Reaction conditions: 473 K, 10 bar H_2, 5 h, 1 g PE, and 0.2 g catalyst.

because otherwise H-MFI-hier30−338 K with open mesopores would have higher solid conversion. Indeed, the rate constant for catalytic cracking of 1,3,5-triisopropylbenzene (TIPB) is 1.2× higher on H-MFI with constricted (NaOH + tetrabutylammonium hydroxide) than open mesopores (NaOH),[50] suggesting that factors other than direct accessibility could also affect solid conversion rates, which will be discussed in further detail at the end of this section. Nonetheless, results herein show that solid conversion rates on hierarchical MFI zeolites are consistently higher than on purely microporous MFI zeolites for all desilication conditions utilized, indicating that improved accessibility to BAS is instrumental in attaining higher conversion rates on medium pore MFI zeolites.

Figure 5b shows lumped gaseous product selectivity and yield obtained from PE upcycling reactions on parent and hierarchical MFI zeolites. The detailed product distribution in terms of both moles and mass are shown in Figures S8 and S9. Gaseous product selectivities on H-MFI-40 and H-MFI-hier15−333 K are similar despite the slight increase in gaseous yield (0.4−0.5 mol % C_1, 20−22 mol % C_2-C_3, 41−42 mol % iso C_4-C_7, and 36−37 mol % linear C_4-C_7) that originates from higher solid conversion obtained on H-MFI-hier15−333 K. Gaseous product selectivities are also similar (0.3 mol % C_1, 16 mol % C_2-C_3, 54−55 mol % iso C_4-C_7, and 29 mol % linear C_4-C_7) on H-MFI-hier30−333 K and H-MFI-hier60−333 K, but the selectivities to iso C_4-C_7 products on these materials are higher than parent H-MFI-40 and H-MFI-hier15−333 K, with concomitant decrease in selectivities to C_2-C_3 and linear C_4-C_7 products. This decrease is not due to differences in solid conversion, since the product selectivities for H-MFI-40 and H-MFI-hier15−333 K remain similar at higher conversions (0.4−0.5 mol % C_1, 22 mol % C_2-C_3, 42 mol % iso C_4-C_7, and 35−36 mol % linear C_4-C_7; Figure S10). Instead, the decrease in selectivities to C_2-C_3 and linear C_4-C_7 products suggests that the larger mesopore volume allows for ingress and egress of bulkier, branched products compared to purely microporous H-MFI-40 and low mesoporosity H-MFI-hier15−333 K. Gaseous product selectivities are within similar ranges (0.2−0.3 mol % C_1, 13−14 mol % C_2-C_3, 61−64 mol % iso C_4-C_7, and 23−26 mol % linear C_4-C_7) on H-MFI-hier30−338 K and H-MFI-hier30−338 K-TPA. This indicates that variations in mesopore connectivities (open or constricted) do not change selectivities toward branched or linear products to a significant extent, despite slight differences in solid conversion. The similarity in gaseous product selectivities also suggests that the constricted mesopores, which are accessible through entrances <4 nm in diameter, are likely still large enough to allow for bulkier, branched hydrocarbons to ingress and egress out of the porous voids, similar to H-MFI-hier30−338 K with open mesopores.

The selectivities to liquid products than to gaseous products on all MFI materials were 3−7× lower by mass (6−16× lower by moles) (Figure S11). The mass of liquid products produced on H-MFI-hierX-333 K (11−14 mg), H-MFI-hier30−338 K (18 mg), and H-MFI-hier30−338 K-TPABr (36 mg) was greater than on parent H-MFI-40 (7 mg), but the product distribution in the C_7-C_{17} range remained similar (Figures S12 and S13). The larger mass of liquid products obtained on hierarchical materials is likely due to both higher attained solid conversions, since the mass of liquid products increased when the solid conversion increased from 14 to 40% on H-MFI-40),[40] and the more rapid egress of longer-chain intermediates without undergoing further beta scission. The amount of aromatics produced on parent and hierarchical MFI catalysts at mild reaction conditions and short reaction times was extremely small, as determined from ^{1}H NMR analysis of the liquid products (Figure S14 and Table S3) and GC-FID of the gaseous products. This is likely due to the presence of H_2 that can hydrogenate alkenes to some extent and the mild reaction conditions used, i.e., short reaction time and low temperature, which is consistent with results from our earlier investigations.[40]

Figure 6a shows that incorporation of mesopores into the FAU framework does not lead to a significant increase in solid conversion and solid conversion rates, in contrast to the results obtained on the MFI framework (Figure 5a). Solid conversions on H-FAU-15-CTA (31%) and H-FAU-15 (33%) were similar, while solid conversion on H-FAU-40-CTA (17%) was lower than H-FAU-40 (27%). The lower solid conversion on H-FAU-40-CTA, despite the large increase in mesopore volume (+285%), could be due to the loss in crystallinity (Figure 1c) and micropore volume (−52%), which accentuates the significance of confinement effects provided by micropores for C−C bond cleavage events through beta scission. However, solid conversions were also similar on parent H-FAU-15 and H-FAU-15-CTA with comparable crystallinity and micropore volume (≤0.05 cm^3 g^{-1}), indicating that mesopore incorporation on H-FAU does not produce the same beneficial effect on solid conversion as observed on H-MFI. This could be due to the larger pore diameters of FAU (~0.74 nm) compared to MFI (~0.56 nm) that allow for easier initial diffusion of the

https://doi.org/10.1021/acscatal.4c01213
ACS Catal. 2024, 14, 7536−7552

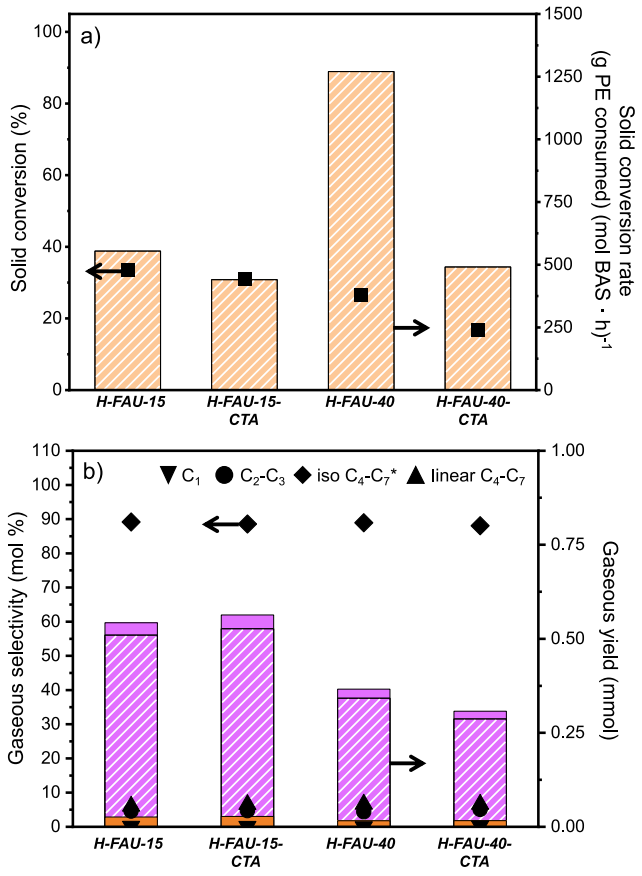

Figure 6. (a) Solid conversion and solid conversion rate and (b) gaseous product selectivity and yield for PE catalytic cracking on parent and hierarchical FAU catalysts. Orange and purple solid bars indicate C_2−C_3 and C_4−C_7 linear alkanes, respectively, while orange and purple striped bars indicate C_1 and C_4−C_7 isoalkanes, respectively. * indicates that C_4−C_7 alkenes are also present and included under this value. Reaction conditions: 473 K, 10 bar H_2, 5 h, 1 g PE, and 0.2 g catalyst.

intermediate products from the PE chain into acid sites within FAU voids compared to MFI, and thus, the increase in solid conversion and solid conversion rate is not as prominent as observed on MFI. Also, this could be a result of higher initial mesopore volumes on parent H-FAU-15 and H-FAU-40 compared to H-MFI-40 due to the steaming and dealumination treatment involved in the synthesis of H-FAU with a high Si/Al ratio. However, since most of these mesopores exist as occluded mesopores,[68,69] we hypothesize that the mesopores should not drastically enhance solid conversion or solid conversion rates. Nonetheless, higher activities of hierarchical FAU zeolites, synthesized under different conditions compared to their commercial parent counterparts with inherent mesopores, have been reported for pyrolysis of PE[52,72] and cracking of TIPB.[72−74] Therefore, it is more likely that the minimal change in solid conversion observed for the experiments described herein is due to the presence of OMM composites. If aluminum atoms are present within the OMM composites due to recrystallization or restructuring of the leached species, the associated acid sites will not be as active for successive C−C bond cleavage events as the parent FAU due to weaker confinement effects. If the aluminum atoms remain within the zeolite framework during desilication due to the presence of CTABr, the OMM formed will likely not contain any aluminum atoms, and consequently, solid conversion on zeolite/OMM composites will be similar or lower than parent zeolites because the surface of the zeolites is covered with silica-based OMM. Taken together, these results show that the presence of a secondary OMM does not significantly enhance catalyst activity, despite larger mesopore volume and retainment of BAS.

Gaseous product selectivities for all parent and hierarchical FAU catalysts were similar (Figure 6b and Figures S15−S17), forming mainly branched C_4−C_7 products (88−89 mol %) with lower selectivity to linear C_4−C_7 (6−7 mol %) and C_2−C_3 (4−5 mol %) products compared to MFI zeolites (Figure 5b). The higher ratio of branched to linear C_4−C_7 products obtained on FAU than on MFI is due to the larger pore diameters of FAU, which can accommodate bulkier reactants or intermediates without subjecting them to secondary isomerization or beta-scission events. This result is also consistent with a larger undulation factor, the ratio of cavity diameter to pore limiting diameter, for FAU compared to MFI, which leads to shorter internal residence times, and consequently, a lesser extent of the oligomerization-cracking cycle.[75,76] Although the selectivity to liquid products on H-FAU was lower than to gaseous products (1−3× lower by mass and 2−6× lower by moles; Figures S18S19), the larger pore diameters on H-FAU led to a higher ratio of liquid to gaseous products and longer liquid hydrocarbon chains than on MFI, consistent with results observed in previous studies.[36,77] Similarly to H-MFI, minimal amounts of aromatics were produced on parent and hierarchical H-FAU (Figure S20 and Table S4), indicating that the differences in the zeolite framework do not drastically change the selectivity to aromatics under mild reaction conditions.

Other factors, such as Lewis acid sites and confinement effects, were also assessed to evaluate whether they impacted the slightly higher conversion rates observed on hierarchical MFI with constricted mesopores (H-MFI-hier30−338 K-TPA) than open mesopores (H-MFI-hier30−338 K). It has been shown that the desilication of microporous zeolites to yield hierarchical zeolites typically increases the density of Lewis acid sites.[78−82] This increase is due to the calcination step following the desilication procedure,[82] which results in minor changes in aluminum coordination (e.g., from tetra- to hexa-coordinated)[82] or dehydroxylation of the BAS.[50,83] The contribution of Lewis acid sites toward cracking (and solid conversion) rates, however, is hard to deconvolute from other concomitant changes (i.e., increase in mesopore volume) to the zeolite after desilication. In one study, catalytic cracking rates of LDPE on lamellar, pillared, nanocrystalline, and hierarchical MFI exhibited a linear dependency on density of BAS but not LAS, which suggest that the contribution of LAS is not as prominent as BAS.[84] Similarly, TGA experiments performed on LLDPE with Al- and Zr-substituted SBA-15 showed that the temperature of maximum PE degradation rate does not correlate with density of LAS.[85] However, LDPE degradation studies performed on Tl- and Ba-loaded BEA[86] and Zr-doped BEA[87] showed lower LDPE decomposition temperature than metal-free BEA, which the authors associate to higher density of LAS within the metal-loaded samples. Within the same study,[86] however, other metal-loaded samples (e.g., Ni, Zn, Sn), which should also have higher density of LAS, have similar or slightly higher LDPE decomposition temperature than parent BEA, but this result was not discussed further. Taken together, contrasting reports on the role of

https://doi.org/10.1021/acscatal.4c01213
ACS Catal. 2024, 14, 7536−7552

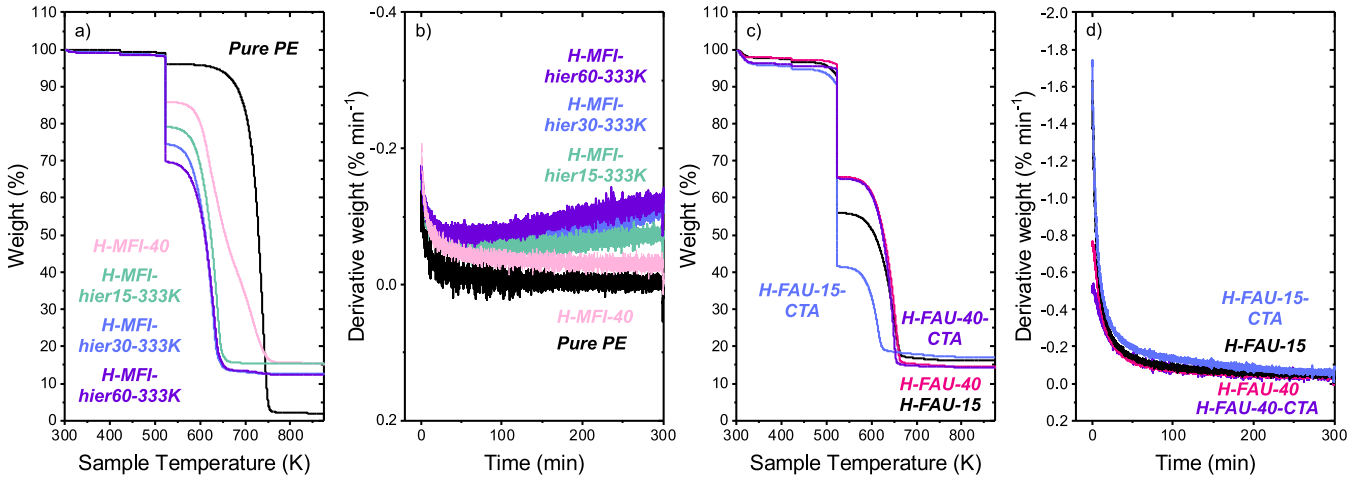

Figure 7. TGA and DTG curves of physical mixtures of PE with (a,b) hierarchical MFI and (c,d) FAU catalysts. Samples were held isothermally at 523 K for 5 h to mimic batch reactor conditions. Time = 0 min on (b) and (d) indicate the time when the system first reached 523 K.

Lewis acid sites exemplify the complexity of isolating the contribution of Lewis acid sites, especially on hierarchical zeolites where the textural properties are also changing.

IR spectra of adsorbed CD_3CN (Figure S21) on parent and hierarchical catalysts within this study show that the ratios of LAS to BAS on hierarchical zeolites are indeed higher than the analogous parent materials. Interestingly, the ratio of LAS to BAS on H-MFI-hier30−338 K-TPA is slightly higher than H-MFI-hier30−338 K (Figure S21a), suggesting that desilication with a surfactant introduces slightly more Lewis acid sites than without surfactant. The higher ratio of LAS to BAS on H-MFI-hier30−338 K-TPA compared to H-MFI-hier30−338 K could potentially contribute to the higher solid conversion rates observed, but H-FAU-15-CTA with higher ratio of LAS to BAS than H-FAU-15 (Figure S21b) does not lead to higher solid conversion rates. Therefore, the exact contribution of Lewis acid sites toward solid conversion rates on hierarchical zeolites remains unclear, but it appears to not be as significant as that of BAS.

The higher solid conversion rate on H-MFI with constricted mesopores relative to open ones could be due to differing confining environments. Indeed, the MFI with constricted mesopores showed a narrower mesopore size distribution (Figure S6) and slightly lower mesopore volume (thus more preserved microporosity; Table 1). Another study revealed that degradation temperatures of PE on desilicated BEA samples were higher than parent BEA, which were argued to be due to weaker confinement in the former, consistent with a lower temperature of ex situ pyridine desorption.[79] Collectively, results in this section show that solid conversion (cracking) rates are not always directly correlated with enhanced accessibility, because there is a trade-off between enhanced accessibility and confinement effects. While the impact of LAS on PE conversion rates would need to be isolated for complete assessment, we propose that the impact of LAS will be less prominent than factors like BAS density, degree of confinement, and site accessibility.

3.3. Solid Conversion Rates Under Flow Conditions via Isothermal Thermogravimetric Analysis. Isothermal thermogravimetric analysis (TGA) under an inert Ar environment was performed to compare trends in solid conversion observed under batch and flow conditions. To minimize safety hazards, Ar was used in place of H_2, which also results in insights that are relevant to pyrolysis of plastic waste with zeolites. TGA under both inert and H_2 environments has been utilized previously to demonstrate the capability of zeolites in lowering the degradation temperature of PE when physically mixed together.[50,88−93] Generally, these thermogravimetric experiments are performed with a linear temperature ramp, e.g., from 293 to 973 K at 10 K min^{-1}, and the respective temperatures at which PE has lost 5%, 50%, and 95% of its initial mass in the presence of different catalysts are compared. In a different approach, we performed isothermal thermogravimetric experiments at 523 K to compare solid conversion rates with those obtained from batch reactions and to analyze trends in the mass loss at a constant temperature as a function of reaction time via derivative thermogravimetry (DTG) curves.

Figure 7 shows the TGA and DTG curves of PE + MFI or FAU catalysts. The trends of solid conversion rates extracted from weight loss curves agree with those from batch experiments (Figure S22), where solid conversion rates were higher on all hierarchical MFI catalysts than on parent MFI. This indicates that the positive impacts of mesopores on solid conversion of hierarchical MFI catalysts hold true regardless of flow conditions and gas types, i.e., H_2 or Ar. Furthermore, solid conversion rates of parent and hierarchical FAU obtained from isothermal thermogravimetric analysis were also similar or lower than parent FAU, consistent with results from batch reactions. We note that the percent weight loss of PE + H-MFI-40 (15%) obtained in this study is lower than that reported in our previous study[40] (40%), because a higher actual temperature set point was used in the previous study due to the use of a different thermocouple, which led to higher conversions. The Curie onset temperature of a new thermocouple matched expected values (Table S1), and all experiments reported herein were performed after a thermocouple replacement.

Solid conversion rates of parent H-FAU were higher than parent H-MFI, which is consistent with a lower initial degradation temperature of PE on H-FAU compared to H-MFI as reported in a previous study with TGA under an H_2 environment.[92] The higher derivative weight losses of PE + zeolites compared to pure PE further highlight the ability of BAS to cleave C−C bonds at modest conditions of <573 K in the absence of metals,[40] which is also supported by an operando study of LDPE on H-MFI that showed formation of

https://doi.org/10.1021/acscatal.4c01213
ACS Catal. 2024, 14, 7536−7552

gaseous products at 503 K.[49] *In situ* ^{1}H MAS NMR was performed on the mixture of PE and H-MFI-40 at reaction temperatures of 350−451 K and reaction times of up to 9 h under an inert N_2 environment (Figure 8) to elucidate the

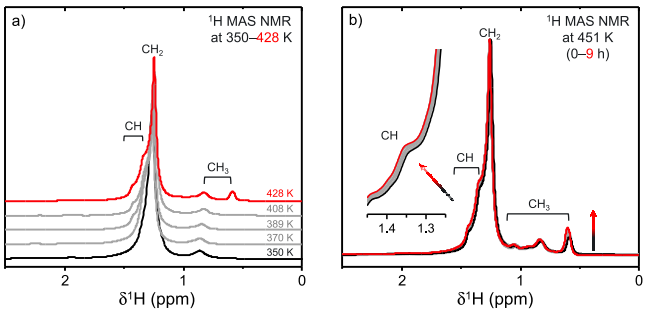

Figure 8. *In situ* ^{1}H MAS NMR on PE with H-MFI-40 (a) at increasing temperatures (350−428 K), and (b) at increasing time (0−9 h) while holding at a constant temperature of 451 K. NMR spectra in (a) are vertically offset for clarity.

structural changes of PE under mild conditions. The intensities of −CH (1.33 ppm) and $-CH_3$ (1.0 and 0.6 ppm) peaks increase (Figure 8a) as the temperature increases from 350 to 451 K and continues to increase when held at 451 K for 9 h (Figure 8b). These increases indicate that polyethylene undergoes isomerization, or a small number of beta-scission events, even at temperatures below those used in the batch and TGA experiments. Isomerization can decrease the reaction temperature required for beta scission because branched alkylcarbenium ions facilitate beta scission at higher rates. It is possible that the lower activation temperature of <523 K could be due to the presence of a small number of weak links within the commercial PE sample utilized in this study, since *in situ* ^{13}C MAS NMR performed on the pure PE alone at 398 K showed features corresponding to the presence of small amounts of −OR and −COOR bonds (Figure S23).

The rates of weight loss remained relatively constant on parent H-MFI (−0.02%), but a gradual increase was observed on hierarchical MFI zeolites over 5 h, from −0.08% at 30 min to −0.13% at 300 min (Figure 7b), indicating that the rate of PE deconstruction increased with time on hierarchical MFI. This increase could be due to (i) higher amounts of branched alkylcarbenium ions formed from isomerization events with increasing reaction time and (ii) greater catalyst stability for hierarchical MFI than for parent MFI. Since beta scission proceeds at a higher rate for substituted alkylcarbenium ions, the rate of C−C bond cleavage should increase if the pool of branched alkylcarbenium ions is larger at longer reaction times, assuming that the catalyst does not undergo any form of deactivation. Given that the DTG curve of H-MFI remained relatively flat across the entire reaction period (Figure 7b), we propose that parent H-MFI deactivates at a higher rate than hierarchical H-MFI during plastic upcycling reactions, and consequently, the larger pool of branched alkylcarbenium ions formed at longer reaction time does not increase C−C cleavage rates further due to limited accessibility to acid sites (or catalyst deactivation). Based on this hypothesis, higher rates of weight loss at longer reaction time on hierarchical MFI zeolites are likely due to the greater catalyst stability of hierarchical MFI, which will be probed in Section 3.4.

Additionally, the similar derivative weight losses between parent H-MFI-40 and hierarchical H-MFI at early time points indicate that the presence of mesopores within MFI materials does not drastically change the rates of initial PE activation or cleavage. This is also likely because the commercial PE utilized in this study is branched (degree of branching = 6.2 mol % C; 62 per 1000 total carbon atoms), as determined from *in situ* ^{13}C NMR at 398 K (Figure S23), which may alter accessibility. Indeed, the degree of branching was previously shown to affect polyethylene cracking, where HDPE with a lower degree of branching (0.7 per 1000 total carbon atoms) was proposed to be able to diffuse into microporous voids of MFI and undergo decomposition, while LLDPE with a higher degree of branching (16.6 per 1000 total carbon atoms) mostly decomposed on surface acid sites.[94] Regardless, the higher solid conversion rates observed on hierarchical MFI materials in this study can be associated with greater weight loss at late time points (Figure 7b), suggesting that the presence of mesopores facilitates more rapid ingress and egress of cleaved fragments from micropores, instead of accelerating initial activation rates.

DTG curves of H-FAU (Figure 7d) are very different from those of H-MFI (Figure 7b). The weight loss rates of H-FAU materials (Figure 7d) are significantly higher than those of H-MFI (Figure 7b) at early time points (<100 min). However, these rates gradually decrease and flatten from −0.03 to −0.09% min^{-1} for H-FAU materials. The higher initial weight losses on H-FAU indicate that PE chains, or large hydrocarbon fragments, can diffuse into the 12-MR windows of FAU zeolite with a higher propensity than for MFI zeolite. Therefore, we expect rate enhancements from mesopore incorporation within large-pore zeolites, e.g., FAU, to be smaller than medium-pore zeolites, e.g., MFI, for polyethylene upcycling, which is consistent with the trends of solid conversion rates obtained within the study described herein. The derivative weight loss of H-FAU-15-CTA is slightly higher than that for H-FAU-15 across all time points (Figure 7d), which indicates that the presence of mesopores, either from intracrystalline or OMMs, without significant destruction of microporous voids can still facilitate both easier ingress and egress of reactants and products. The DTG curves of H-FAU-40 and H-FAU-40-CTA, however, are similar (Figure 7d). This similarity can be associated with a significant reduction in the ratios of micropore to mesopore volume (Table 1), where the ability of interconnected mesopores within H-FAU-40-CTA to alleviate diffusion limitations is counteracted by weaker confinement effects in the mesoporous regions.

3.4. Impact of Mesopores on Catalyst Stability and Coke Accumulation. Given that the above data indicate differences in stability afforded by the different porous structures, presumably through differences in the accumulation of carbonaceous deposits, isothermal thermogravimetric experiments (Figure 7) were further analyzed to provide important insights into rates of deactivation. Despite the higher solid conversion rates on H-FAU, the DTG curves of H-FAU (Figure 7d) show a steeper decrease over time than H-MFI (Figure 7b), indicating that H-FAU deactivates at a higher rate. This is consistent with more rapid coke formation and formation of bulkier polycyclic aromatic species that remain lodged within the micropores on H-FAU compared to that on H-MFI due to the larger pore diameters of H-FAU, as reported in previous studies.[95−97] Furthermore, the similar derivative weight losses of H-FAU and H-MFI at long reaction times of >1.5 h show that the higher solid conversion rates obtained on

https://doi.org/10.1021/acscatal.4c01213
ACS Catal. 2024, 14, 7536−7552

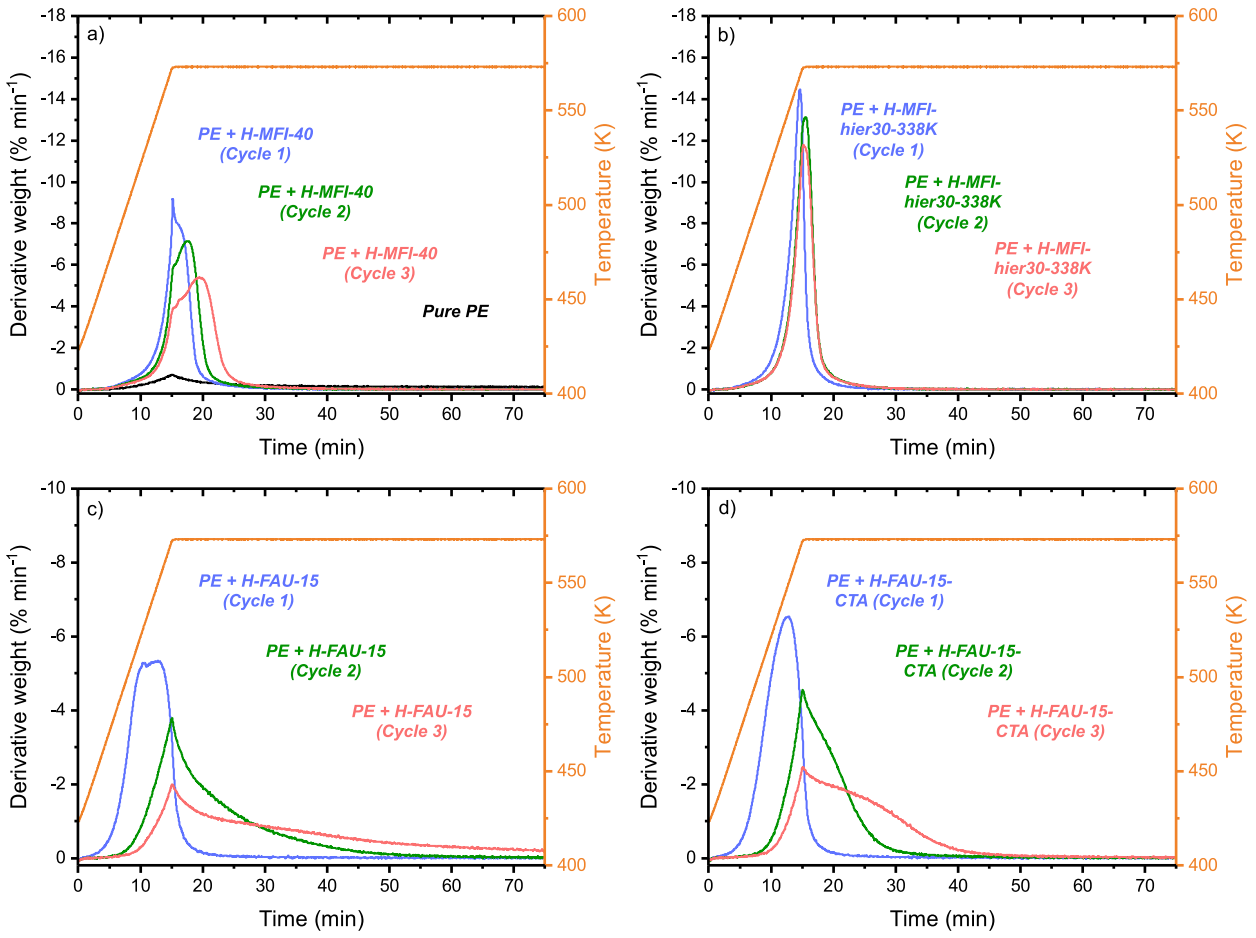

Figure 9. Derivative weight loss curves of (a) PE + H-MFI-40, (b) PE + H-MFI-hier30−338 K, (c) PE + H-FAU-15, and (d) PE + H-FAU-15-CTA for each recyclability cycle. Samples were held isothermally at 573 K for 1 h to allow for 100% PE conversion. Time = 0 min on all figures indicates the time when the system started ramping the temperature from 423 to 573 K.

H-FAU are due to the higher initial rates of PE cracking and not prolonged catalyst lifetime.

Recyclability experiments were performed on the suite of parent and hierarchical zeolites to further evaluate how the incorporation of mesopores into microporous zeolites impacts catalyst stability. Catalyst recyclability was initially probed by batch reactions at a higher reaction temperature of 498 K and at an extended reaction time of 17 h to yield only the spent catalysts after 100% solid conversion for PE upcycling reactions (no solvent washing was used for catalyst recovery). The solid conversion on H-MFI-40 remained at 100% after the first two runs but decreased to 54% after the third run (Figure S24), which concurrently agrees with the buildup of heavier coke on the catalyst surface or within the micropores after successive runs, as measured by TGA of the spent catalysts (Figure S25). However, on H-FAU-15, solid conversion only increased from 33% to 53% despite the higher temperature and longer reaction time (Figure S24). This restricts further batch recyclability experiments on H-FAU materials, because the recovered catalyst is intimately mixed with either unreacted or shorter-chain PE, masking the actual mass of the catalyst loaded for subsequent recyclability runs. Moreover, probing catalyst stability by using one data point at an extremely long reaction time may lead to incorrect conclusions about catalyst stability and recyclability,[98,99] since the catalyst might have been able to attain 100% solid conversion within the designated reaction time despite significant catalyst deactivation.

To circumvent these issues, additional recyclability experiments were performed using TGA. Figures S26−S29 show the weight loss curves and solid conversion rates of parent and hierarchical MFI and FAU after three cycles. Each cycle consisted of an isothermal hold at 573 K for 1 h, which was sufficient to attain 100% solid conversion even after three cycles on parent H-MFI and H-FAU materials. The solid conversion rates on the suite of parent and hierarchical catalysts remained similar across all three cycles (Figures S28 and S29) which suggests that both the parent and hierarchical materials do not undergo significant deactivation at first sight. However, the DTG curves from the recyclability experiments (Figures 9 and S30) show that most of the PE fully degraded within the first 25 min, and consequently, the solid conversion rates do not decrease across the three cycles when normalized by the reaction time of 1 h despite changes in the degradation rates.

The shifts in the absolute maxima of the derivative weight loss curves toward longer time points (Figures 9 andS30) show that all the catalysts do in fact undergo deactivation, but to differing extents. For instance, the maximum point of the weight loss curve gradually shifts from 15.2 min (first cycle) to 19.5 min (third cycle) on H-MFI-40, with a concomitant increase in the fwhm of the curve from 4.2 min (first cycle) to 7.6 min (third cycle). The increase in the fwhm indicates that a

https://doi.org/10.1021/acscatal.4c01213
ACS Catal. 2024, 14, 7536−7552

longer reaction time is required to fully degrade PE on the spent MFI catalyst. These results strongly demonstrate that the PE chains take longer to access both surface and internal BAS of parent H-MFI-40 following multiple cycles, which is due to formation of coke that restricts access to these active sites. The shifts in the maximum points (<0.7 min) on H-MFI-hier30−338 K and H-MFI-hier30−338 K-TPA are much smaller than that of H-MFI-40 after three cycles, with a very small increase in fwhm (<0.6 min). These results indicate that the catalyst stability and recyclability of hierarchical MFI zeolites surpasses that of the parent MFI zeolite. This is likely due to the presence of mesopores that can prolong accessibility of cleaved fragments to micropores despite the occurrence of gradual pore blockage. The fwhm values of hierarchical MFI (2.9−3.5 min) are also smaller than those of H-MFI-40 (4.2−7.6 min), consistent with the higher solid conversion rates observed on hierarchical MFI samples (Figure S22).

The maximum point of the DTG curve for H-FAU-15 also shifts to a later time point (from 12 to 15.2 min, Figure 9c) after each cycle, similar to that observed on parent H-MFI-40 (Figure 9a). A similar shift can be seen with H-FAU-15-CTA across the cycles (from 12.7 to 15.1 min), but the slopes of the initial onset (from 7.5 to 15 min) of cycles 2 and 3 on H-FAU-15-CTA are steeper than those on H-FAU-15, and the fwhm value on H-FAU-15-CTA is smaller than that on H-FAU-15. These results show that mesopores, either intracrystalline or from OMM, are still able to facilitate easier ingress of reactants in the presence of coke on H-FAU, which is consistent with the results presented in Section 3.3, but to a lesser extent than that observed on hierarchical H-MFI due to the larger amount of coke accumulated within FAU. Interestingly, the maximum points of H-FAU-40 and H-FAU-40-CTA do not shift across cycles (Figure S30c), which is due in part to slower initial degradation of these materials in the first cycle compared to that on H-FAU-15 and H-FAU-15-CTA. The slower initial degradation can be attributed to the lower density of BAS on H-FAU-40 and H-FAU-40-CTA compared to H-FAU-15 and H-FAU-15-CTA. Despite similarities in the maximum points of the DTG curves across cycles, the initial onsets for cycles 2 and 3 on H-FAU-40 and H-FAU-40-CTA were shifted to later time points (Figure S30c), indicating catalyst deactivation. In general, the fwhm values of the DTG curves across all cycles for H-FAU-40-CTA are greater than for H-FAU-40. This difference can be attributed to weaker confinement effects on H-FAU-40-CTA due to formation of ordered mesoporous materials and a loss of crystallinity that prolongs the residence time needed for beta scission.

The amount of coke accumulated on catalysts after PE conversion was determined through combustion of the spent catalysts after isothermal and recyclability TGA runs. After the isothermal runs, the mass ratios of coke to loaded catalyst for hierarchical MFI, with the exception of H-MFI-hier30−338 K-TPA, and FAU zeolites were 1.3−2.3× lower than their parent counterparts (Figure 10), indicating less coke accumulation on hierarchical zeolites after one PE degradation run. However, the mass ratio of coke to loaded catalyst for H-MFI-hier30−338 K-TPA was similar to parent H-MFI, which shows that constricted mesopores are more vulnerable to coke accumulation than open mesopores on MFI catalysts. This observation is consistent with an earlier study that shows larger amounts of olefinic and aromatic species formed within H-MFI desilicated with TBAOH, which forms constricted mesopores, compared to parent H-MFI after polyethylene degradation.[49]

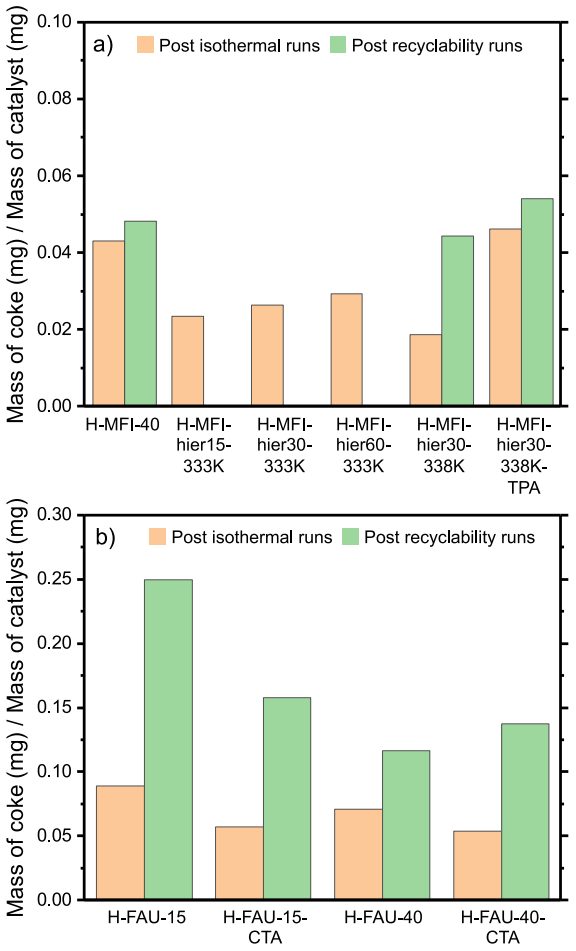

Figure 10. Mass ratios of coke to catalyst determined from TGA experiments for parent and hierarchical (a) MFI and (b) FAU catalysts.

The trends for mass ratios of coke to loaded catalyst after recyclability runs (green bars; Figure 10) differ slightly from those after isothermal runs (orange bars; Figure 10), since the catalysts from the recyclability runs are subjected to three 1 h PE reaction cycles at a higher temperature of 573 K instead of one 5 h isothermal run at 523 K. The mass ratios of coke to catalyst after the recyclability runs were similar for parent and hierarchical MFI (H-MFI-hier30−338 K and H-MFI-hier30−338 K-TPA; Figure 10a), suggesting that the absolute amount of coke that can be amassed on these materials are similar, differing only by ∼1.2×. Therefore, the greater catalyst stability observed on hierarchical MFI materials from recyclability runs is not the result of a smaller total amount of coke formed, but rather, due to the retained accessibility of reactants to active acid sites despite the presence of coke. This is similar to results we observed using benzyl alcohol-trimethylbenzene alkylation as a probe reaction.[100] Interestingly, the mass ratio of coke to catalyst on H-FAU-15-CTA was 1.6× lower than that on H-FAU-15, but the mass ratios of coke to catalyst on H-FAU-40 and H-FAU-40-CTA were similar, differing by ∼1.2×. We hypothesize that the presence of OMM leads to a higher absolute quantity of carbonaceous species formed due to the larger pore sizes, but the presence of intracrystalline mesopores within FAU can also lead to more rapid egress of bulkier molecules, which reduces coke accumulation. Therefore, H-FAU-15-CTA, with higher ratios of intracrystalline mesopores

https://doi.org/10.1021/acscatal.4c01213
ACS Catal. 2024, 14, 7536−7552

to OMMs compared to H-FAU-40-CTA, accumulates less coke than H-FAU-40-CTA after three cycles.

Collectively, results from this section show that catalyst stability cannot be accurately probed by comparing solid conversion rates across different cycles in batch reactions unless the exact point of time at which the catalyst reaches 100% solid conversion in the first cycle is known. Therefore, the utilization of thermogravimetric analysis is more suitable to probe catalyst stability, since the rate of PE weight loss can be obtained. Generally, the presence of intracrystalline mesopores will lead to higher catalyst stability regardless of the zeolite framework, but mesopores from OMM within zeolite/OMM composites do not increase catalyst stability due to the associated larger carbonaceous accumulations.

4. CONCLUSION

Solid conversion rates of polyethylene obtained from batch and isothermal TGA reactions are systematically higher on hierarchical than parent MFI samples regardless of desilication conditions, e.g., desilication time, temperature, and with or without TPABr, but solid conversion rates on hierarchical FAU synthesized via desilication with CTABr are similar or lower compared to parent FAU despite increases in mesopore volume. These comparisons reveal that the introduction of mesopores into conventionally microporous zeolites does not always enhance conversion rates. Instead, conversion rates exhibit complex dependencies on the identity and quality of mesopores formed, confinement effects rendered by micropores, and the pore diameters of the parent zeolite framework. The solid conversion rates of hierarchical FAU samples do not surpass those of parent FAU, because the mesopores formed are from both intracrystalline mesopores and ordered mesoporous materials. This composite structure results from the presence of CTA^+ that facilitates recrystallization of leached species. Additionally, since a larger portion of the PE chain can access micropores of parent FAU compared to MFI, based on the larger initial weight losses from TGA reactions, the relative increase in solid conversion rates from mesopore incorporation within large pore zeolites is less significant than that for medium pore zeolites. Regardless, recyclability experiments show that hierarchical MFI and FAU catalysts with intracrystalline mesopores (and not from ordered mesoporous materials) have better catalyst stability than their parent counterparts, highlighting the beneficial impact of these mesopores in mitigating catalyst deactivation. Overall, the data presented in the studies reported herein demonstrate that the incorporation of mesopores into microporous MFI structures can result in enhanced conversion rate and improved catalyst stability, while composites of hierarchical FAU zeolites and ordered mesoporous materials do not substantially enhance conversion rates due to weaker confinement effects.

■ ASSOCIATED CONTENT

Supporting Information

The Supporting Information is available free of charge at https://pubs.acs.org/doi/10.1021/acscatal.4c01213.

Characterization of parent and hierarchical zeolites, thermogravimetric curves, solid conversion rates, gaseous and liquid product distributions, and nuclear magnetic resonance spectroscopy data (PDF)

■ AUTHOR INFORMATION

Corresponding Author

Michele L. Sarazen − *Department of Chemical and Biological Engineering, Princeton University, Princeton, New Jersey 08544, United States;* orcid.org/0000-0002-5732-7130; Email: msarazen@princeton.edu

Authors

Jun Zhi Tan − *Department of Chemical and Biological Engineering, Princeton University, Princeton, New Jersey 08544, United States;* orcid.org/0000-0002-9643-2232

Maaso Ortega − *Department of Chemical and Biological Engineering, Princeton University, Princeton, New Jersey 08544, United States*

Sophia A. Miller − *Department of Chemical and Biological Engineering, Princeton University, Princeton, New Jersey 08544, United States*

Cole W. Hullfish − *Department of Chemical and Biological Engineering, Princeton University, Princeton, New Jersey 08544, United States;* orcid.org/0000-0001-6804-0517

Hojoon Kim − *Department of Chemical and Biological Engineering, Princeton University, Princeton, New Jersey 08544, United States*

Sungmin Kim − *Institute for Integrated Catalysis, Pacific Northwest National Laboratory, Richland, Washington 99352, United States;* orcid.org/0000-0001-6602-1320

Wenda Hu − *The Gene & Linda Voiland School of Chemical Engineering and Bioengineering, Washington State University, Pullman, Washington 99164, United States*

Jian Zhi Hu − *Institute for Integrated Catalysis, Pacific Northwest National Laboratory, Richland, Washington 99352, United States; The Gene & Linda Voiland School of Chemical Engineering and Bioengineering, Washington State University, Pullman, Washington 99164, United States;* orcid.org/0000-0001-8879-747X

Johannes A. Lercher − *Institute for Integrated Catalysis, Pacific Northwest National Laboratory, Richland, Washington 99352, United States; Department of Chemistry and Catalysis Research Center, Technische Universität München, Garching 85748, Germany;* orcid.org/0000-0002-2495-1404

Bruce E. Koel − *Department of Chemical and Biological Engineering, Princeton University, Princeton, New Jersey 08544, United States;* orcid.org/0000-0002-0032-4991

Complete contact information is available at: https://pubs.acs.org/10.1021/acscatal.4c01213

Notes

The authors declare no competing financial interest.

■ ACKNOWLEDGMENTS

This work was supported by the U.S. Department of Energy, Office of Basic Energy Sciences through a subcontract from PNNL (FWP 78459). M.O. acknowledges support from the Office of Undergraduate Research Student Initiated Internship Program (OURSIP). S.A.M acknowledges support from the Peter B. Lewis Fund for Student Innovation in Energy and the Environment and the LENS Funding Initiative. C.W.H. acknowledges partial support from the National Science Foundation Graduate Research Fellowship (NSF DGE-2039656). H.K. acknowledges support from the High Meadows Environmental Institute's Undergraduate Research

Fund, DuPont Senior Thesis Fellowship Grant in memory of Michelle Goudie '93, and the School of Engineering and Applied Science Senior Thesis Fund. We acknowledge the partial support from the High Meadows Environmental Institute Grand Challenge Award and use of Princeton's Imaging and Analysis Center, which is partially supported through the Princeton Center for Complex Materials (PCCM), a National Science Foundation (NSF)-MRSEC program (DMR-2011750). *In situ* ^{13}C and ^{1}H MAS NMR experiments were supported by the U.S. Department of Energy, Office of Basic Energy Sciences, Division of Chemical Sciences, Geosciences, and Biosciences within the Catalysis Science Program (FWP 47319). We thank Hayat Adawi for helpful comments and discussion on the manuscript, and Denis Potapenko and John Schreiber at the Princeton Imaging and Analysis Center for providing training and helpful assistance on instruments.

REFERENCES

(1) Andrady, A. L.; Neal, M. A. Applications and Societal Benefits of Plastics. *Philos. Trans. R. Soc. B Biol. Sci.* **2009**, *364*, 1977−1984.
(2) Nava, V.; Chandra, S.; Aherne, J.; Alfonso, M. B.; Antão-Geraldes, A. M.; Attermeyer, K.; Bao, R.; Bartrons, M.; Berger, S. A.; Biernaczyk, M.; et al.et al. Plastic Debris in Lakes and Reservoirs. *Nature* **2023**, *619* (7969), 317−322.
(3) Pinheiro, H. T.; MacDonald, C.; Santos, R. G.; Ali, R.; Bobat, A.; Cresswell, B. J.; Francini-Filho, R.; Freitas, R.; Galbraith, G. F.; Musembi, P.; et al.etal. Plastic Pollution on the World's Coral Reefs. *Nature* **2023**, *619* (7969), 311−316.
(4) Bucci, K.; Tulio, M.; Rochman, C. M. What Is Known and Unknown about the Effects of Plastic Pollution: A Meta-Analysis and Systematic Review. *Ecol. Appl.* **2020**, *30* (2), No. e02044.
(5) Turner, A.; Arnold, R.; Williams, T. Weathering and Persistence of Plastic in the Marine Environment: Lessons from LEGO. *Environ. Pollut.* **2020**, *262*, 114299.
(6) Chamas, A.; Moon, H.; Zheng, J.; Qiu, Y.; Tabassum, T.; Jang, J. H.; Abu-Omar, M.; Scott, S. L.; Suh, S. Degradation Rates of Plastics in the Environment. *ACS Sustainable Chem. Eng.* **2020**, *8* (9), 3494−3511.
(7) Krause, S.; Molari, M.; Gorb, E. V.; Gorb, S. N.; Kossel, E.; Haeckel, M. Persistence of Plastic Debris and Its Colonization by Bacterial Communities after Two Decades on the Abyssal Seafloor. *Sci. Rep.* **2020**, *10* (1), 9484.
(8) Ter Halle, A.; Ghiglione, J. F. Nanoplastics: A Complex, Polluting Terra Incognita. *Environ. Sci. Technol.* **2021**, *55* (21), 14466−14469.
(9) Li, H.; Aguirre-Villegas, H. A.; Allen, R. D.; Bai, X.; Benson, C. H.; Beckham, G. T.; Bradshaw, S. L.; Brown, J. L.; Brown, R. C.; Cecon, V. S.; et al.et al. Expanding Plastics Recycling Technologies: Chemical Aspects, Technology Status and Challenges. *Green Chem.* **2022**, *24* (23), 8899−9002.
(10) Garcia, J. M.; Robertson, M. L. The Future of Plastics Recycling. *Science* **2017**, *358* (6365), 870−872.
(11) Schyns, Z. O. G.; Shaver, M. P. Mechanical Recycling of Packaging Plastics: A Review. *Macromol. Rapid Commun.* **2021**, *42* (3), 2000415.
(12) Ragaert, K.; Delva, L.; Van Geem, K. Mechanical and Chemical Recycling of Solid Plastic Waste. *Waste Manag.* **2017**, *69*, 24−58.
(13) Civancik-Uslu, D.; Nhu, T. T.; Van Gorp, B.; Kresovic, U.; Larrain, M.; Billen, P.; Ragaert, K.; De Meester, S.; Dewulf, J.; Huysveld, S. Moving from Linear to Circular Household Plastic Packaging in Belgium: Prospective Life Cycle Assessment of Mechanical and Thermochemical Recycling. *Resour. Conserv. Recycl.* **2021**, *171*, 105633.
(14) Khoo, H. H. LCA of Plastic Waste Recovery into Recycled Materials, Energy and Fuels in Singapore. *Resour. Conserv. Recycl.* **2019**, *145*, 67−77.
(15) Venkatachalam, V.; Pohler, M.; Spierling, S.; Nickel, L.; Barner, L.; Endres, H.-J. Design for Recycling Strategies Based on the Life Cycle Assessment and End of Life Options of Plastics in a Circular Economy. *Macromol. Chem. Phys.* **2022**, *223* (13), 2200046.
(16) Wu, C.; Williams, P. T. Pyrolysis−Gasification of Plastics, Mixed Plastics and Real-World Plastic Waste with and without Ni−Mg−Al Catalyst. *Fuel* **2010**, *89* (10), 3022−3032.
(17) Lee, K.; Jing, Y.; Wang, Y.; Yan, N. A Unified View on Catalytic Conversion of Biomass and Waste Plastics. *Nat. Rev. Chem.* **2022**, *6* (9), 635−652.
(18) Al-Asadi, M.; Miskolczi, N.; Eller, Z. Pyrolysis-Gasification of Wastes Plastics for Syngas Production Using Metal Modified Zeolite Catalysts under Different Ratio of Nitrogen/Oxygen. *J. Cleaner Prod.* **2020**, *271*, 122186.
(19) Tan, K. Q.; Ahmad, M. A.; Oh, W. D.; Low, S. C. Valorization of Hazardous Plastic Wastes into Value-Added Resources by Catalytic Pyrolysis-Gasification: A Review of Techno-Economic Analysis. *Renew. Sustain. Energy Rev.* **2023**, *182*, 113346.
(20) Shah, H. H.; Amin, M.; Iqbal, A.; Nadeem, I.; Kalin, M.; Soomar, A. M.; Galal, A. M. A Review on Gasification and Pyrolysis of Waste Plastics. *Front. Chem.* **2023**, *10*, 960894.
(21) Sastre, G.; Corma, A. The Confinement Effect in Zeolites. *J. Mol. Catal. A: chem.* **2009**, *305* (1), 3−7.
(22) Bhan, A.; Gounder, R.; Macht, J.; Iglesia, E. Entropy Considerations in Monomolecular Cracking of Alkanes on Acidic Zeolites. *J. Catal.* **2008**, *253* (1), 221−224.
(23) Noh, G.; Shi, Z.; Zones, S. I.; Iglesia, E. Isomerization and β-Scission Reactions of Alkanes on Bifunctional Metal-Acid Catalysts: Consequences of Confinement and Diffusional Constraints on Reactivity and Selectivity. *J. Catal.* **2018**, *368*, 389−410.
(24) Sarazen, M. L.; Doskocil, E.; Iglesia, E. Catalysis on Solid Acids: Mechanism and Catalyst Descriptors in Oligomerization Reactions of Light Alkenes. *J. Catal.* **2016**, *344*, 553−569.
(25) Jones, A. J.; Zones, S. I.; Iglesia, E. Implications of Transition State Confinement within Small Voids for Acid Catalysis. *J. Phys. Chem. C* **2014**, *118* (31), 17787−17800.
(26) Gounder, R.; Iglesia, E. The Catalytic Diversity of Zeolites: Confinement and Solvation Effects within Voids of Molecular Dimensions. *Chem. Commun.* **2013**, *49* (34), 3491−3509.
(27) Noh, G.; Zones, S. I.; Iglesia, E. Consequences of Acid Strength and Diffusional Constraints for Alkane Isomerization and β-Scission Turnover Rates and Selectivities on Bifunctional Metal-Acid Catalysts. *J. Phys. Chem. C* **2018**, *122* (44), 25475−25497.
(28) Hullfish, C. W.; Tan, J. Z.; Adawi, H. I.; Sarazen, M. L. Toward Intrinsic Catalytic Rates and Selectivities of Zeolites in the Presence of Limiting Diffusion and Deactivation. *ACS Catal.* **2023**, *13* (19), 13140−13150.
(29) Feliczak-Guzik, A. Hierarchical Zeolites: Synthesis and Catalytic Properties. *Microporous Mesoporous Mater.* **2018**, *259*, 33−45.
(30) Pérez-Ramírez, J.; Christensen, C. H.; Egeblad, K.; Christensen, C. H.; Groen, J. C. Hierarchical Zeolites: Enhanced Utilisation of Microporous Crystals in Catalysis by Advances in Materials Design. *Chem. Soc. Rev.* **2008**, *37* (11), 2530−2542.
(31) Hartmann, M.; Machoke, A. G.; Schwieger, W. Catalytic Test Reactions for the Evaluation of Hierarchical Zeolites. *Chem. Soc. Rev.* **2016**, *45* (12), 3313−3330.
(32) Chen, L.-H.; Sun, M.-H.; Wang, Z.; Yang, W.; Xie, Z.; Su, B.-L. Hierarchically Structured Zeolites: From Design to Application. *Chem. Rev.* **2020**, *120* (20), 11194−11294.
(33) Mallette, A. J.; Seo, S.; Rimer, J. D. Synthesis Strategies and Design Principles for Nanosized and Hierarchical Zeolites. *Nat. Synth.* **2022**, *1* (7), 521−534.
(34) Peng, P.; Gao, X.-H.; Yan, Z.-F.; Mintova, S. Diffusion and Catalyst Efficiency in Hierarchical Zeolite Catalysts. *Natl. Sci. Rev.* **2020**, *7* (11), 1726−1742.
(35) Han, X.; Zhou, X.; Ji, T.; Zeng, F.; Deng, W.; Tang, Z.; Chen, R. Boosting the Catalytic Performance of Metal−Zeolite Catalysts in

https://doi.org/10.1021/acscatal.4c01213
ACS Catal. 2024, 14, 7536−7552

the Hydrocracking of Polyolefin Wastes by Optimizing the Nanoscale Proximity. *EES Catal.* **2024**, *2* (1), 300−310.
(36) Liu, S.; Kots, P. A.; Vance, B. C.; Danielson, A.; Vlachos, D. G. Plastic Waste to Fuels by Hydrocracking at Mild Conditions. *Sci. Adv.* **2021**, *7* (17), No. eabf8283.
(37) Rorrer, J. E.; Ebrahim, A. M.; Questell-Santiago, Y.; Zhu, J.; Troyano-Valls, C.; Asundi, A. S.; Brenner, A. E.; Bare, S. R.; Tassone, C. J.; Beckham, G. T.; et al.et al. Role of Bifunctional Ru/Acid Catalysts in the Selective Hydrocracking of Polyethylene and Polypropylene Waste to Liquid Hydrocarbons. *ACS Catal.* **2022**, *12*, 13969−13979.
(38) Kots, P. A.; Vance, B. C.; Vlachos, D. G. Polyolefin Plastic Waste Hydroconversion to Fuels, Lubricants, and Waxes: A Comparative Study. *React. Chem. Eng.* **2021**, *7* (1), 41−54.
(39) Bin Jumah, A.; Anbumuthu, V.; Tedstone, A. A.; Garforth, A. A. Catalyzing the Hydrocracking of Low Density Polyethylene. *Ind. Eng. Chem. Res.* **2019**, *58* (45), 20601−20609.
(40) Tan, J. Z.; Hullfish, C. W.; Zheng, Y.; Koel, B. E.; Sarazen, M. L. Conversion of Polyethylene Waste to Short Chain Hydrocarbons under Mild Temperature and Hydrogen Pressure with Metal-Free and Metal-Loaded MFI Zeolites. *Appl. Catal. B Environ.* **2023**, *338*, 123028.
(41) Hittinger, J. P.; Shantz, D. F. Systematic Study of Low Temperature Cracking of Low-Density Polyethylene with ZSM-5. *Microporous Mesoporous Mater.* **2022**, *343*, 112170.
(42) Tsubota, S.; Kokuryo, S.; Tamura, K.; Miyake, K.; Uchida, Y.; Mizusawa, A.; Kubo, T.; Nishiyama, N. Exploring the Effect of Brønsted Acidity of MFI-Type Zeolites on Catalytic Cracking Temperature of Low Density Polyethylene. *Catal. Sci. Technol.* **2024**, *14*, 1369.
(43) Duan, J.; Chen, W.; Wang, C.; Wang, L.; Liu, Z.; Yi, X.; Fang, W.; Wang, H.; Wei, H.; Xu, S.; et al.et al. Coking-Resistant Polyethylene Upcycling Modulated by Zeolite Micropore Diffusion. *J. Am. Chem. Soc.* **2022**, *144* (31), 14269−14277.
(44) Lee, J. Y.; Park, S. M.; Saha, S. K.; Cho, S. J.; Seo, G. Liquid-Phase Degradation of Polyethylene (PE) over MFI Zeolites with Mesopores: Effects of the Structure of PE and the Characteristics of Mesopores. *Appl. Catal. B Environ.* **2011**, *108*−*109*, 61−71.
(45) Serrano, D. P.; Aguado, J.; Escola, J. M. Developing Advanced Catalysts for the Conversion of Polyolefinic Waste Plastics into Fuels and Chemicals. *ACS Catal.* **2012**, *2* (9), 1924−1941.
(46) Song, G.; Chen, W.; Dang, P.; Yang, S.; Zhang, Y.; Wang, Y.; Xiao, R.; Ma, R.; Li, F. Synthesis and Characterization of Hierarchical ZSM-5 Zeolites with Outstanding Mesoporosity and Excellent Catalytic Properties. *Nanoscale Res. Lett.* **2018**, *13* (1), 364.
(47) Munir, D.; Usman, M. R. Mesoporous HZSM-5 Catalysts for the Conversion of Waste Plastics to Liquid Fuels. *J. Porous Mater.* **2022**, *29* (3), 783−794.
(48) Tarach, K. A.; Pyra, K.; Góra-Marek, K. Opening up ZSM-5 Hierarchical Zeolite's Porosity through Sequential Treatments for Improved Low-Density Polyethylene Cracking. *Molecules* **2020**, *25*, 2878.
(49) Tarach, K. A.; Pyra, K.; Siles, S.; Melián-Cabrera, I.; Góra-Marek, K. Operando Study Reveals the Superior Cracking Activity and Stability of Hierarchical ZSM-5 Catalyst for the Cracking of Low-Density Polyethylene. *ChemSuschem* **2019**, *12* (3), 633−638.
(50) Tarach, K. A.; Góra-Marek, K.; Martinez-Triguero, J.; Melián-Cabrera, I. Acidity and Accessibility Studies of Desilicated ZSM-5 Zeolites in Terms of Their Effectiveness as Catalysts in Acid-Catalyzed Cracking Processes. *Catal. Sci. Technol.* **2017**, *7* (4), 858−873.
(51) Thibault-Starzyk, F.; Stan, I.; Abelló, S.; Bonilla, A.; Thomas, K.; Fernandez, C.; Gilson, J.-P.; Pérez-Ramírez, J. Quantification of Enhanced Acid Site Accessibility in Hierarchical Zeolites − The Accessibility Index. *J. Catal.* **2009**, *264* (1), 11−14.
(52) Verboekend, D.; Vilé, G.; Pérez-Ramírez, J. Hierarchical Y and USY Zeolites Designed by Post-Synthetic Strategies. *Adv. Funct. Mater.* **2012**, *22* (5), 916−928.
(53) Mingorance-Baena, A.; Siles-Quesada, S.; Tarach, K.; Morales, M. V.; Gora-Marek, K.; Melián-Cabrera, I. Improved Catalytic Technology for Waste Plastic Processing: Toward Novel Remediation and Emission Control Measures. *ACS Sustainable Chem. Eng.* **2019**, *7* (1), 129−133.
(54) Groen, J. C.; Peffer, L. A. A.; Moulijn, J. A.; Pérez-Ramírez, J. Mechanism of Hierarchical Porosity Development in MFI Zeolites by Desilication: The Role of Aluminium as a Pore-Directing Agent. *Chem. − A Eur. J.* **2005**, *11* (17), 4983−4994.
(55) Groen, J. C.; Peffer, L. A. A.; Moulijn, J. A.; Pérez-Ramírez, J. Mesoporosity Development in ZSM-5 Zeolite upon Optimized Desilication Conditions in Alkaline Medium. *Colloids Surfaces A Physicochem. Eng. Asp.* **2004**, *241* (1), 53−58.
(56) Milina, M.; Mitchell, S.; Crivelli, P.; Cooke, D.; Pérez-Ramírez, J. Mesopore Quality Determines the Lifetime of Hierarchically Structured Zeolite Catalysts. *Nat. Commun.* **2014**, *5* (1), 3922.
(57) Kresnawahjuesa, O.; Gorte, R. J.; de Oliveira, D.; Lau, L. Inexpensive, and Reliable Method for Measuring Brønsted-Acid Site Densities in Solid Acids. *Catal. Lett.* **2002**, *82* (3), 155−160.
(58) Abdelrahman, O. A.; Vinter, K. P.; Ren, L.; Xu, D.; Gorte, R. J.; Tsapatsis, M.; Dauenhauer, P. J. Simple Quantification of Zeolite Acid Site Density by Reactive Gas Chromatography. *Catal. Sci. Technol.* **2017**, *7* (17), 3831−3841.
(59) Biaglow, A. I.; Parrillo, D. J.; Gorte, R. J. Characterization of H,Na-Y Using Amine Desorption. *J. Catal.* **1993**, *144* (1), 193−201.
(60) Palkhiwala, A. G.; Gorte, R. J. Characterization of H-FER and H-TON Using Temperature-Programmed Desorption of Alkylamines. *Catal. Lett.* **1999**, *57* (1), 19−23.
(61) Hu, J. Z.; Hu, M. Y.; Zhao, Z.; Xu, S.; Vjunov, A.; Shi, H.; Camaioni, D. M.; Peden, C. H. F.; Lercher, J. A. Sealed Rotors for in Situ High Temperature High Pressure MAS NMR. *Chem. Commun.* **2015**, *51* (70), 13458−13461.
(62) Jaegers, N. R.; Mueller, K. T.; Wang, Y.; Hu, J. Z. Variable Temperature and Pressure Operando MAS NMR for Catalysis Science and Related Materials. *Acc. Chem. Res.* **2020**, *53* (3), 611−619.
(63) Jaegers, N. R.; Hu, W.; Wang, Y.; Hu, J. Z. High-Temperature and High-Pressure In Situ Magic Angle Spinning Nuclear Magnetic Resonance Spectroscopy. *JoVE* **2020**, No. 164, No. e61794.
(64) Verboekend, D.; Vilé, G.; Pérez-Ramírez, J. Mesopore Formation in USY and Beta Zeolites by Base Leaching: Selection Criteria and Optimization of Pore-Directing Agents. *Cryst. Growth Des.* **2012**, *12* (6), 3123−3132.
(65) Verboekend, D.; Milina, M.; Mitchell, S.; Pérez-Ramírez, J. Hierarchical Zeolites by Desilication: Occurrence and Catalytic Impact of Recrystallization and Restructuring. *Cryst. Growth Des.* **2013**, *13* (11), 5025−5035.
(66) Groen, J. C.; Jansen, J. C.; Moulijn, J. A.; Pérez-Ramírez, J. Optimal Aluminum-Assisted Mesoporosity Development in MFI Zeolites by Desilication. *J. Phys. Chem. B* **2004**, *108* (35), 13062−13065.
(67) Thommes, M.; Mitchell, S.; Pérez-Ramírez, J. No Title. *J. Phys. Chem. C* **2012**, *116*, 18816.
(68) Kortunov, P.; Vasenkov, S.; Kärger, J.; Valiullin, R.; Gottschalk, P.; Fé Elía, M.; Perez, M.; Stöcker, M.; Drescher, B.; McElhiney, G.; et al.et al. The Role of Mesopores in Intracrystalline Transport in USY Zeolite: PFG NMR Diffusion Study on Various Length Scales. *J. Am. Chem. Soc.* **2005**, *127* (37), 13055−13059.
(69) Janssen, A. H.; Koster, A. J.; de Jong, K. P. On the Shape of the Mesopores in Zeolite Y: A Three-Dimensional Transmission Electron Microscopy Study Combined with Texture Analysis. *J. Phys. Chem. B* **2002**, *106* (46), 11905−11909.
(70) Gu, J.; Lin, J.; Smith, A. J.; Soontaranon, S.; Rugmai, S.; Kongmark, C.; Coppens, M.-O.; Sankar, G. Towards Understanding Mesopore Formation in Zeolite Y Crystals Using Alkaline Additives via in Situ Small-Angle X-Ray Scattering. *Microporous Mesoporous Mater.* **2022**, *338*, 111867.
(71) Zholobenko, V.; Freitas, C.; Jendrlin, M.; Bazin, P.; Travert, A.; Thibault-Starzyk, F. Probing the Acid Sites of Zeolites with Pyridine:

https://doi.org/10.1021/acscatal.4c01213
ACS Catal. 2024, 14, 7536−7552

Quantitative AGIR Measurements of the Molar Absorption Coefficients. *J. Catal.* **2020**, *385*, 52−60.
(72) Mensah, J.; Yan, P.; Rawal, A.; Lee, A. F.; Wilson, K.; Robinson, N.; Johns, M. L.; Kennedy, E.; Stockenhuber, M. Catalytic Cracking of 1,3,5-Triisopropylbenzene and Low-Density Polyethylene over Hierarchical Y Zeolites and Al-SBA-15. *ChemCatchem* **2024**, *16* (3), No. e202300884.
(73) Ying, J. Y.; Garcia-Martinez, J. Mesostructured Zeolitic Materials, and Methods of Making and Using the Same. U.S US 20,050,239,634 A1, 2005.
(74) Ying, J. Y.; Garcia-Martinez, J. Mesostructured Zeolitic Materials, and Methods of Making and Using the Same. U.S US 20,050,239,634 A1, 2009.
(75) Sarazen, M. L.; Doskocil, E.; Iglesia, E. Effects of Void Environment and Acid Strength on Alkene Oligomerization Selectivity. *ACS Catal.* **2016**, *6* (10), 7059−7070.
(76) Biscardi, J. A.; Iglesia, E. Structure and Function of Metal Cations in Light Alkane Reactions Catalyzed by Modified H-ZSM5. *Catal. Today* **1996**, *31* (3), 207−231.
(77) Wang, Y.; Zhang, Y.; Fan, H.; Wu, P.; Liu, M.; Li, X.; Yang, J.; Liu, C.; Bai, P.; Yan, Z. Elucidating the Structure-Performance Relationship of Typical Commercial Zeolites in Catalytic Cracking of Low-Density Polyethylene. *Catal. Today* **2022**, *405*−*406*, 135−143.
(78) Tarach, K. A.; Martinez-Triguero, J.; Valencia, S.; Wojciechowska, K.; Rey, F.; Góra-Marek, K. Hierarchical Zeolites TNU-9 and IM-5 as the Catalysts for Cracking Processes. *Appl. Catal. B Environ.* **2023**, *338*, 123066.
(79) Pyra, K.; Tarach, K. A.; Majda, D.; Góra-Marek, K. Desilicated Zeolite BEA for the Catalytic Cracking of LDPE: The Interplay between Acidic Sites' Strength and Accessibility. *Catal. Sci. Technol.* **2019**, *9* (8), 1794−1801.
(80) Dapsens, P. Y.; Mondelli, C.; Pérez-Ramírez, J. Highly Selective Lewis Acid Sites in Desilicated MFI Zeolites for Dihydroxyacetone Isomerization to Lactic Acid. *ChemSuschem* **2013**, *6* (5), 831−839.
(81) Verboekend, D.; Mitchell, S.; Milina, M.; Groen, J. C.; Pérez-Ramírez, J. Full Compositional Flexibility in the Preparation of Mesoporous MFI Zeolites by Desilication. *J. Phys. Chem. C* **2011**, *115* (29), 14193−14203.
(82) Mitchell, S.; Milina, M.; Verel, R.; Hernández-Rodríguez, M.; Pinar, A. B.; McCusker, L. B.; Pérez-Ramírez, J. Aluminum Redistribution during the Preparation of Hierarchical Zeolites by Desilication. *Chem. − A Eur. J.* **2015**, *21* (40), 14156−14164.
(83) Sadowska, K.; Góra-Marek, K.; Drozdek, M.; Kuśtrowski, P.; Datka, J.; Martinez Triguero, J.; Rey, F. Desilication of Highly Siliceous Zeolite ZSM-5 with NaOH and NaOH/Tetrabutylamine Hydroxide. *Microporous Mesoporous Mater.* **2013**, *168*, 195−205.
(84) Peral, A.; Escola, J. M.; Serrano, D. P.; Řech, J.; Ochoa-Hernández, C.; čejka, J. Bidimensional ZSM-5 Zeolites Probed as Catalysts for Polyethylene Cracking. *Catal. Sci. Technol.* **2016**, *6* (8), 2754−2765.
(85) Finelli, V.; Gentilin, V.; Mossotti, G.; Ricchiardi, G.; Piovano, A.; Crocellà, V.; Groppo, E. The Role of Porosity and Acidity in the Catalytic Upcycling of Polyethylene. *Catal. Today* **2023**, *419*, 114142.
(86) Kokuryo, S.; Tamura, K.; Miyake, K.; Uchida, Y.; Mizusawa, A.; Kubo, T.; Nishiyama, N. LDPE Cracking over Mono- and Divalent Metal-Doped Beta Zeolites. *Catal. Sci. Technol.* **2022**, *12* (13), 4138−4144.
(87) Kokuryo, S.; Miyake, K.; Uchida, Y.; Tanaka, S.; Miyamoto, M.; Oumi, Y.; Mizusawa, A.; Kubo, T.; Nishiyama, N. Design of Zr- and Al-Doped *BEA-Type Zeolite to Boost LDPE Cracking. *ACS Omega.* **2022**, *7* (15), 12971−12977.
(88) Coelho, A.; Costa, L.; Marques, M. M.; Fonseca, I. M.; Lemos, M. A. N. D. A.; Lemos, F. The Effect of ZSM-5 Zeolite Acidity on the Catalytic Degradation of High-Density Polyethylene Using Simultaneous DSC/TG Analysis. *Appl. Catal. A Gen.* **2012**, *413*−*414*, 183−191.
(89) Coelho, A.; Fonseca, I. M.; Matos, I.; Marques, M. M.; Botelho Do Rego, A. M.; Lemos, M. A. N. D. A.; Lemos, F. Catalytic Degradation of Low and High Density Polyethylenes Using Ethylene Polymerization Catalysts: Kinetic Studies Using Simultaneous TG/DSC Analysis. *Appl. Catal. A Gen.* **2010**, *374* (1), 170−179.
(90) Caldeira, V. P. S.; Santos, A. G. D.; Oliveira, D. S.; Lima, R. B.; Souza, L. D.; Pergher, S. B. C. Polyethylene Catalytic Cracking by Thermogravimetric Analysis. *J. Therm. Anal. Calorim.* **2017**, *130* (3), 1939−1951.
(91) Manos, G.; Garforth, A.; Dwyer, J. Catalytic Degradation of High-Density Polyethylene on an Ultrastable-Y Zeolite. Nature of Initial Polymer Reactions, Pattern of Formation of Gas and Liquid Products, and Temperature Effects. *Ind. Eng. Chem. Res.* **2000**, *39* (5), 1203−1208.
(92) Costa, C. S.; Muñoz, M.; Ribeiro, M. R.; Silva, J. M. H-USY and H-ZSM-5 Zeolites as Catalysts for HDPE Conversion under a Hydrogen Reductive Atmosphere. *Sustain. Energy Fuels* **2021**, *5* (4), 1134−1147.
(93) Costa, C. S.; Muñoz, M.; Ribeiro, M. R.; Silva, J. M. A Thermogravimetric Study of HDPE Conversion under a Reductive Atmosphere. *Catal. Today* **2021**, *379*, 192−204.
(94) Jerdy, A. C.; Trevisi, L.; Monwar, M.; González-Borja, M. Á.; Abbott, R.; Lobban, L.; Crossley, S. Deconvoluting the Roles of Polyolefin Branching and Unsaturation on Depolymerization Reactions over Acid Catalysts. *Appl. Catal. B Environ.* **2023**, *337*, 122986.
(95) Marcilla, A.; Gómez-Siurana, A.; Valdés, F. J. Evolution of the Deactivation Mode and Nature of Coke of HZSM-5 and USY Zeolites in the Catalytic Cracking of Low-Density Polyethylene during Successive Cracking Runs. *Appl. Catal. A Gen.* **2009**, *352* (1), 152−158.
(96) Castaño, P.; Elordi, G.; Olazar, M.; Aguayo, A. T.; Pawelec, B.; Bilbao, J. Insights into the Coke Deposited on HZSM-5, Hβ and HY Zeolites during the Cracking of Polyethylene. *Appl. Catal. B Environ.* **2011**, *104* (1), 91−100.
(97) Elordi, G.; Olazar, M.; Lopez, G.; Castaño, P.; Bilbao, J. Role of Pore Structure in the Deactivation of Zeolites (HZSM-5, Hβ and HY) by Coke in the Pyrolysis of Polyethylene in a Conical Spouted Bed Reactor. *Appl. Catal. B Environ.* **2011**, *102* (1), 224−231.
(98) Scott, S. L. A Matter of Life(Time) and Death. *ACS Catal.* **2018**, *8* (9), 8597−8599.
(99) Bligaard, T.; Bullock, R. M.; Campbell, C. T.; Chen, J. G.; Gates, B. C.; Gorte, R. J.; Jones, C. W.; Jones, W. D.; Kitchin, J. R.; Scott, S. L. Toward Benchmarking in Catalysis Science: Best Practices, Challenges, and Opportunities. *ACS Catal.* **2016**, *6* (4), 2590−2602.
(100) Adawi, H. I.; Zheng, Y.; Sarazen, M. L. Underpinnings of Carbonaceous Deposition among Structurally Diverse Hierarchical Zeolites during Hydrocarbon Upgrading. *Cryst. Growth Des.* **2023**, *23* (4), 2675−2688.

https://doi.org/10.1021/acscatal.4c01213
ACS Catal. 2024, 14, 7536−7552